AD-A112 112 NAVAL RESEARCH LAB WASHINGTON DC F/G 14/2
AN AEROSOL CHAMBER FOR PULSED DF LASER PROPAGATION EFFECTS STUD--ETC(U)
FEB 82 G L TRUSTY, T H COSDEN, D H LESLIE
UNCLASSIFIED NRL-MR-4738 NL

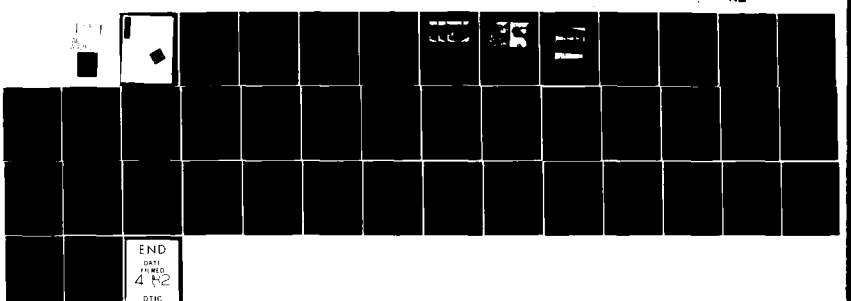

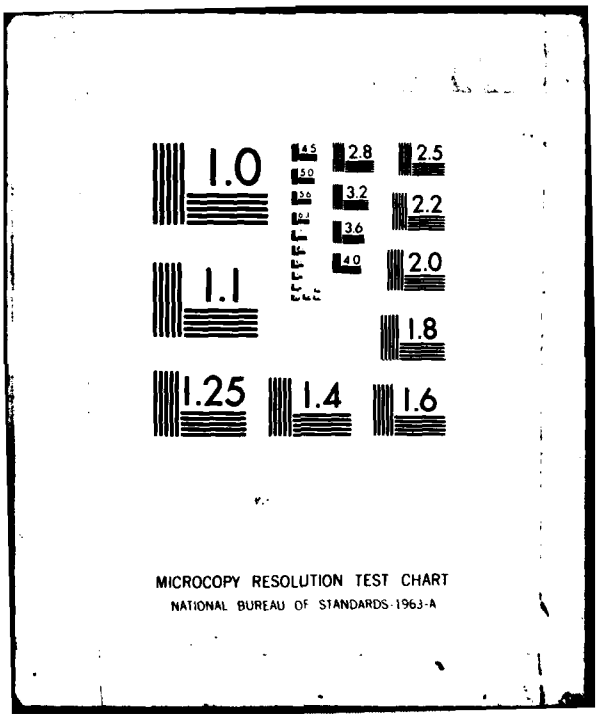
1.0
1.1
1.25
1.4
1.6
1.8
2.0
2.2
2.5
2.8
3.2
3.6
4.0
MICROCOPY RESOLUTION TEST CHART
NATIONAL BUREAU OF STANDARDS-1963-A

SECURITY CLASSIFICATION OF THIS PAGE (When Data Entered)

REPORT DOCUMENTATION PAGE	READ INSTRUCTIONS BEFORE COMPLETING FORM
1. REPORT NUMBER: NRL Memorandum Report 4738 — 2. GOVT ACCESSION NO.: AD-A112 112	3. RECIPIENT'S CATALOG NUMBER:
4. TITLE (and Subtitle): AN AEROSOL CHAMBER FOR PULSED DF LASER PROPAGATION EFFECTS STUDIES	5. TYPE OF REPORT & PERIOD COVERED: Interim 6. PERFORMING ORG. REPORT NUMBER:
7. AUTHOR(s): Gary L. Trusty, Thomas H. Cosden, and Daniel H. Leslie	8. CONTRACT OR GRANT NUMBER(s):
9. PERFORMING ORGANIZATION NAME AND ADDRESS: Naval Research Laboratory, Washington, DC 20375	10. PROGRAM ELEMENT, PROJECT, TASK AREA & WORK UNIT NUMBERS: 627 35N, RF35-388-800, 65-1171-00
11. CONTROLLING OFFICE NAME AND ADDRESS: Naval Research Laboratory, Washington, DC 20375	12. REPORT DATE: February 4, 1982 13. NUMBER OF PAGES: 41
14. MONITORING AGENCY NAME & ADDRESS (if different from Controlling Office)	15. SECURITY CLASS. (of this report): UNCLASSIFIED 15a. DECLASSIFICATION/DOWNGRADING SCHEDULE:

16. DISTRIBUTION STATEMENT (of this Report)

Approved for public release; distribution unlimited

17. DISTRIBUTION STATEMENT (of the abstract entered in Block 20, if different from Report)

18. SUPPLEMENTARY NOTES

19. KEY WORDS (Continue on reverse side if necessary and identify by block number)

Air breakdown
DF laser
Pulsed laser
Aerosol generation
Aerosol measurement

20. ABSTRACT (Continue on reverse side if necessary and identify by block number)

For performing an aerosol-induced air-breakdown experiment at 3.8 μm we put together a facility for generating an aerosol and monitoring the particle size distribution. We describe the facility and its performance during the breakdown experiment.

DD FORM 1 JAN 73 1473 EDITION OF 1 NOV 65 IS OBSOLETE
S/N 0102-014-6601

SECURITY CLASSIFICATION OF THIS PAGE (When Data Entered)

CONTENTS

AN AEROSOL CHAMBER FOR PULSED DF LASER PROPAGATION EFFECTS STUDIES

THE PROBLEM

Air breakdown is a phenomenon associated with high peak power density of a high-energy laser pulse during atmospheric transmission. When the local EM fields are large enough clean air will ionize, creating a plasma. The threshold for clean-air breakdown is about 10^{10} watts/cm^2 at 3.8 μm and one atmosphere pressure. Introducing particulates into the air reduces the threshold condsiderably (several orders of magnitude). The threshold reduction is a function of the wavelength of radiation and the size of the particulates.[1] For shipboard use of a high-energy laser, sea spray and salt-laden aerosols may greatly reduce the device effectiveness because the plasma at the breakdown site is opaque to laser radiation, thus preventing energy from reaching the target. Hence it is necessary to understand the relationship between breakdown threshold and particulate size and makeup so that high-energy pulsed laser operation in the marine environment can be properly assessed.

Studies of aerosol-induced air breakdown have been done at 10.6 μm for several kinds of artifically created particles.[2] As part of a joint effort between NRL and The Aerospace Corporation, we report here a portion of the first breakdown study done at 3.8 μm.

In this experiment Aerospace provided the laser, the optics and the optical diagnostics equipment. NRL provided the aerosol generation (chamber included), the diagnostic tools for monitoring the aerosol, and the equipment and software for reducing and displaying the particle size distributions. This report describes NRL's part of this joint experiment.

Manuscript submitted December 9, 1981.

THE APPROACH

Our previous measurements of naturally-occurring marine aerosols at both open-sea and coastal locations give us a good idea of the range of aerosol size distributions to expect.[3,4] Our approach here was to create an aerosol similar to a naturally-occurring distribution and fire a pulsed DF laser through it, monitoring the breakdown phenomenon as a function of a laser power density and aerosol size distribution.

We used Particle Measuring Systems, Inc. (PMS) particle spectrometers to monitor the particle size distribution. These are the same instruments we used many times to measure the natural aerosols in the marine environment and the procedure for using them in an open-air situation is familiar and straight-forward.

If one creates an aerosol in a chamber, however, then measures the particles by drawing air samples from that chamber, the particle count could be depleted quite quickly. To prevent the loss of generated aerosol particles we used a large container (7 × 7 × 12 feet) with both the aerosol generators and the aerosol spectrometers inside. Small motor-driven doors at each end allowed the laser beam to enter and exit the box. A similar long narrow slot opened lengthwise on the box for optical monitoring of the breakdown.

The aerosol generator and breakdown box were fabricated at the Chesapeake Bay Division (CBD) of NRL. Since the laser was located at The Aerospace Corporation in El Segundo, California, for the breakdown experiment we transported the box and associated electronics to the Aerospace site.

THE AEROSOL BREAKDOWN BOX

The box was a standard military "Helio-Hut" to which we made several major modifications. Figure 1 shows a view of the outside of the aerosol box from the access-door end. Figures 1a and 1b show the box with the laser exit door closed and open respectively. In Figure 1c the cover for the clear-air filter is shown open.

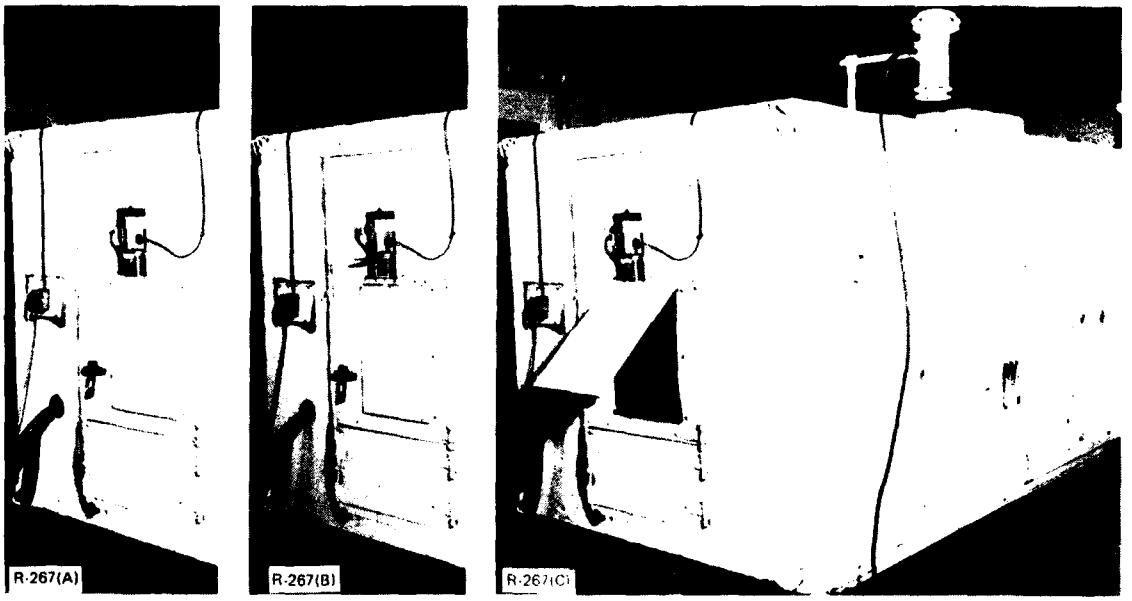

Fig. 1 — An end view of the aerosol breakdown box

Figure 2 shows the inside of the box viewed through the access door. In the back wall are two exhaust fans, which, in conjunction with the air filter allow us to reduce the background particle count to a negligible level. The filter is an Astrocel model manufactured by American Air Filter Corporation and is rated as 99% efficient at 0.3 μm and between 80 and 90% efficient at 0.1 μm. The edge of the door-mounted air filter can be seen in the right foreground. Also seen in Fig. 2 inside the box are the particle spectrometers, an EG&G Model 110 air temperature/dew point set, and two types of water-droplet generators.

There are three particle spectrometers, all manufactured by PMS. The Active Scattering Aerosol Spectrometer Probe (ASASP) measures the small particles (0.13-0.75 μm), the High Volume version of the Classical Scattering Aerosol Spectrometer Probe (CSASP-HV) measures the mid-range particles (0.75-15 μm), and the Optical Array Probe (OAP) covers the very large particles (10-150 μm). (All particle sizes referenced here will be in terms of radius.) A data acquisition system accesses all three probes and the air temperature/dew point set simultaneously with one-second time resolution.

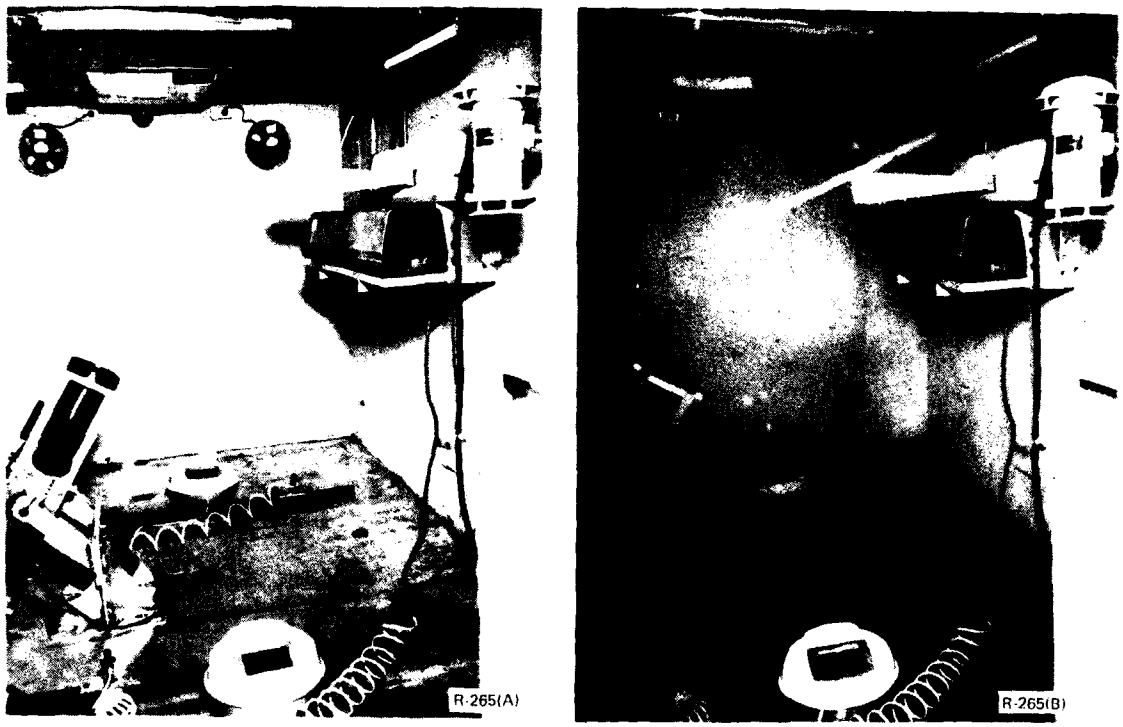

(a) (b)

Fig. 2 — Inside the aerosol box with and without the particle generators operating

For droplet generation there are four high-pressure fog nozzles. Each has its own valve to allow control over steady-state generation. The nozzles are type OC10 manufactured by Bete Fog Nozzle, Inc. We use the fog nozzles primarily for initial raising of the relative humidity inside the box as well as providing one type of size distribution. We then have the option of switching to the two spinning-disc generators for a different size distribution. These generators are Montgomery Ward Cool Mist Vaporizers. Figure 2b shows the droplet generators running, with a HeNe probe laser illuminating the optical path. Measurements from start-up showed a constant distribution was attained in 20 minutes or so, and remained constant until shut-down.

After the particles have been generated, the fast-acting motor-driven doors over each of the openings allow a negligible loss of particles during the laser firing. Figures 3a and 3b show the viewing slots on the side of the box with the doors closed and open, respectively.

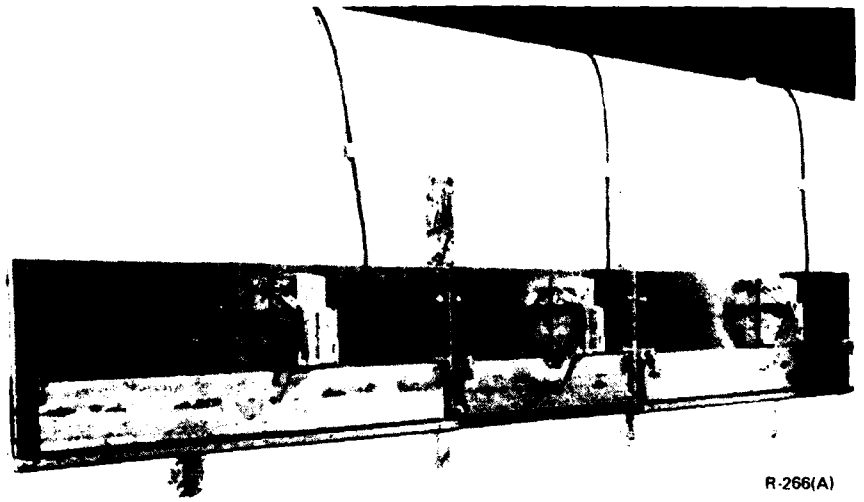

(a)

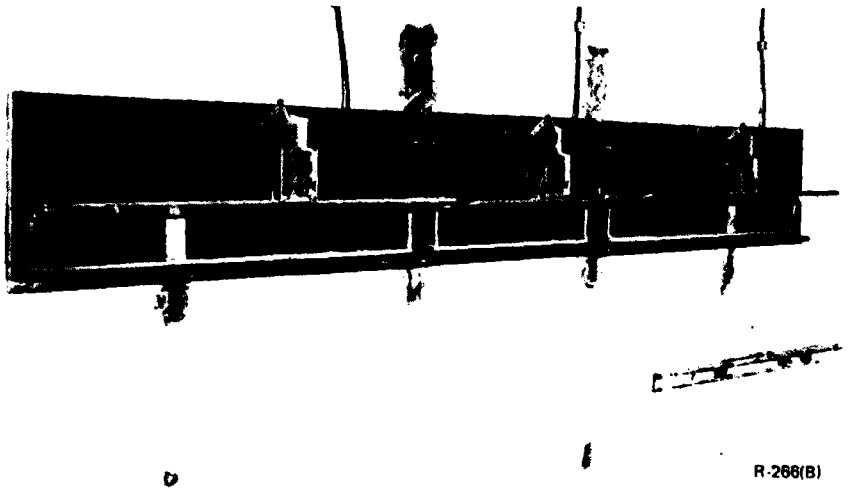

(b)

Fig. 3 — The side viewing ports on the aerosol box: opened and closed

The PMS Data Acquisition System stores the aerosol-particle size counts and analog data on 9-track magnetic tape. Simultaneously, the data is directed to a PDP 11/34 computer for real-time processing. For displaying and analyzing our ambient aerosol data we have developed a rather elaborate collection of software.[5] As an example, Fig. 4 is a plot of a measured aerosol-particle size distribution of a natural aerosol obtained at CBD prior to shipping the equipment to California. The box was sitting outdoors in the full sun with the exhaust fans running and the doors open, hence, the high inside temperature (AT1) and the lower inside relative humidity (RH1). AT2 and RH2 are the outside air temperature and relative humidity. (The outside EG&G device could be seen in Fig. 1c.) Figure 5 shows the resultant size distribution after closing the door, turning off the exhaust fans, and letting all four fog nozzles run full throttle for about 20 minutes.

The aerosol software allows post-processing of the magnetic tape as well as real-time processing. The last two figures came from creating a file of 5-minute averages from the tape. In those figures we see that the relative humidity increased considerably when the nozzles were turned on. To observe that variation we can take advantage of another data display capability which allows any stored variable to be plotted versus any other variable, or any variable as a function of time.

Figure 6 shows the relative humidity plotted versus times for three hours of that test at CBD. Here we have taken data from a 1-minute-average file. A slightly rising but stable background value exists until the nozzles were turned on at 1424. The humidity then rises immediately until the nozzles were shut off at 1435, where it fails until the nozzles were opened ten minutes later. The relative humidity reached saturation by 1500 hours, when the Fig. 5 data occurred. (Note that in that figure RH1 shows a value of over 100%. This does not imply supersaturation. The relative humidity is continuously calculated from the dew point and air temperatures, and near saturation a value of 101% is within the error of those measurements.) About 1510 the nozzles were shut off and the relative humidity slowly dropped until 1540 when the exhaust fans were turned on and the door was opened.

Figure 7 shows the particle size distribution at 1515, not long after nozzle shut-off. A comparison with Fig. 5 shows that most of the large particles are gone.

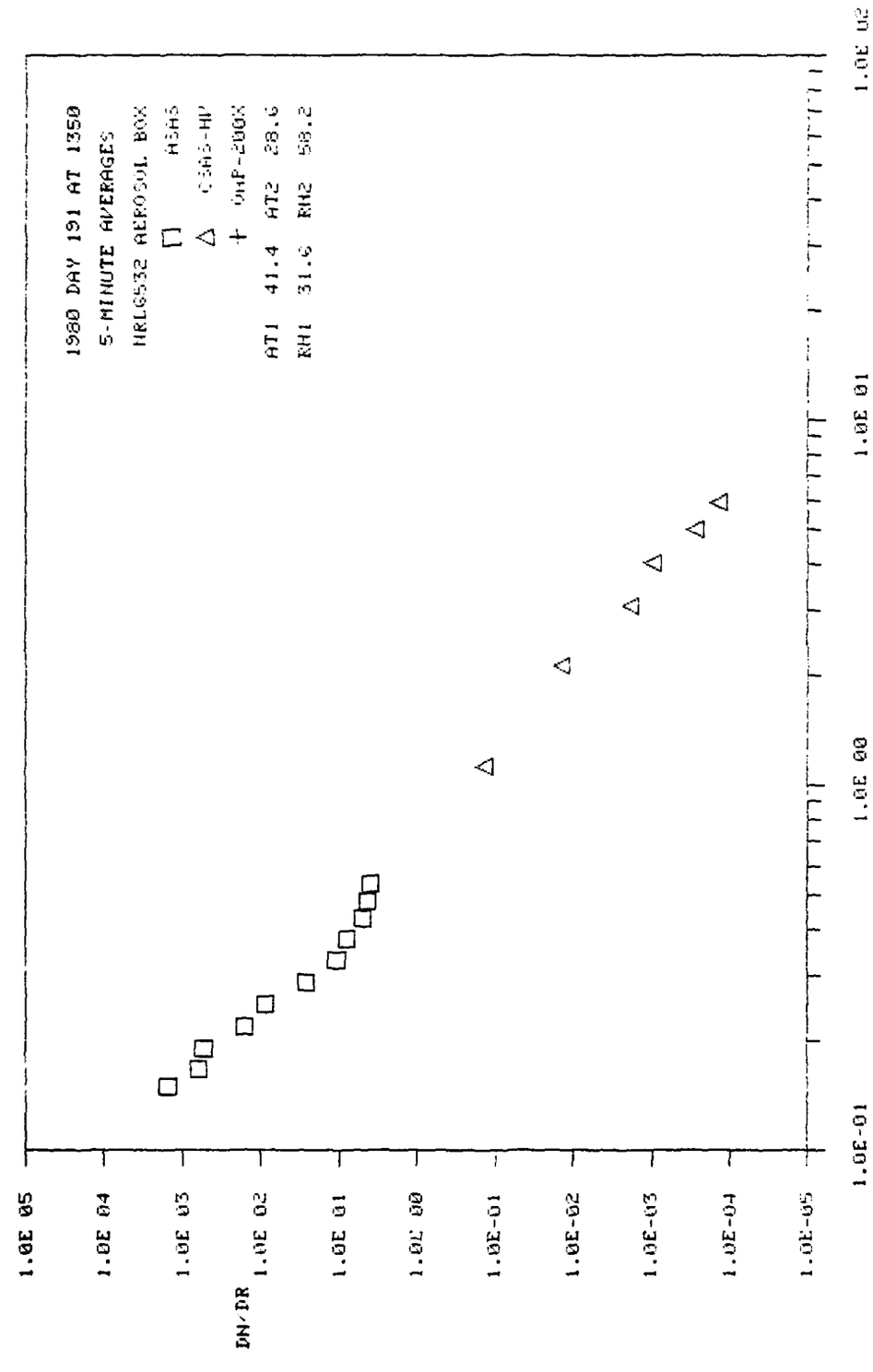

Fig. 4 — An ambient aerosol-particle size distribution

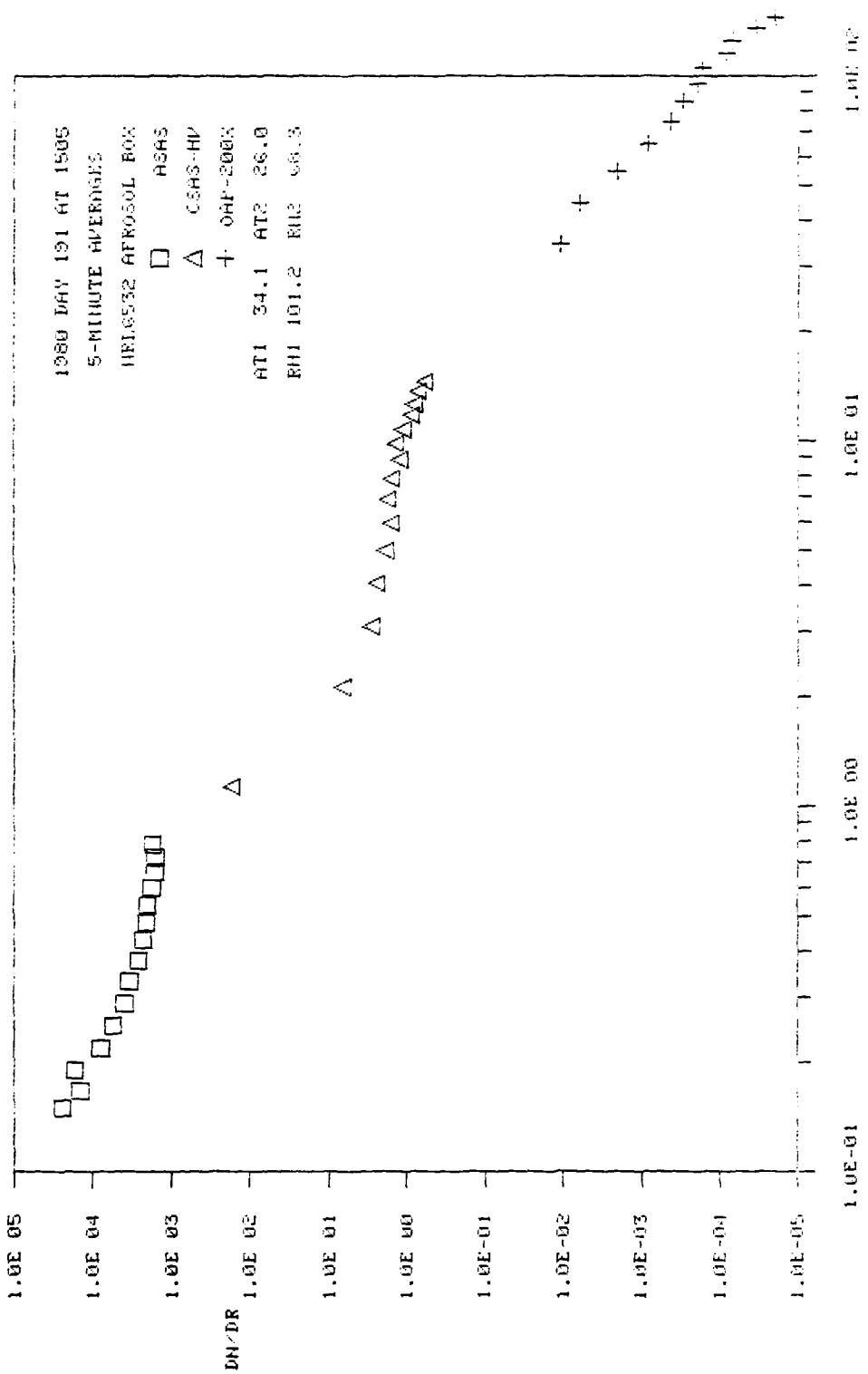

Fig. 5 — A generated aerosol-particle size distribution

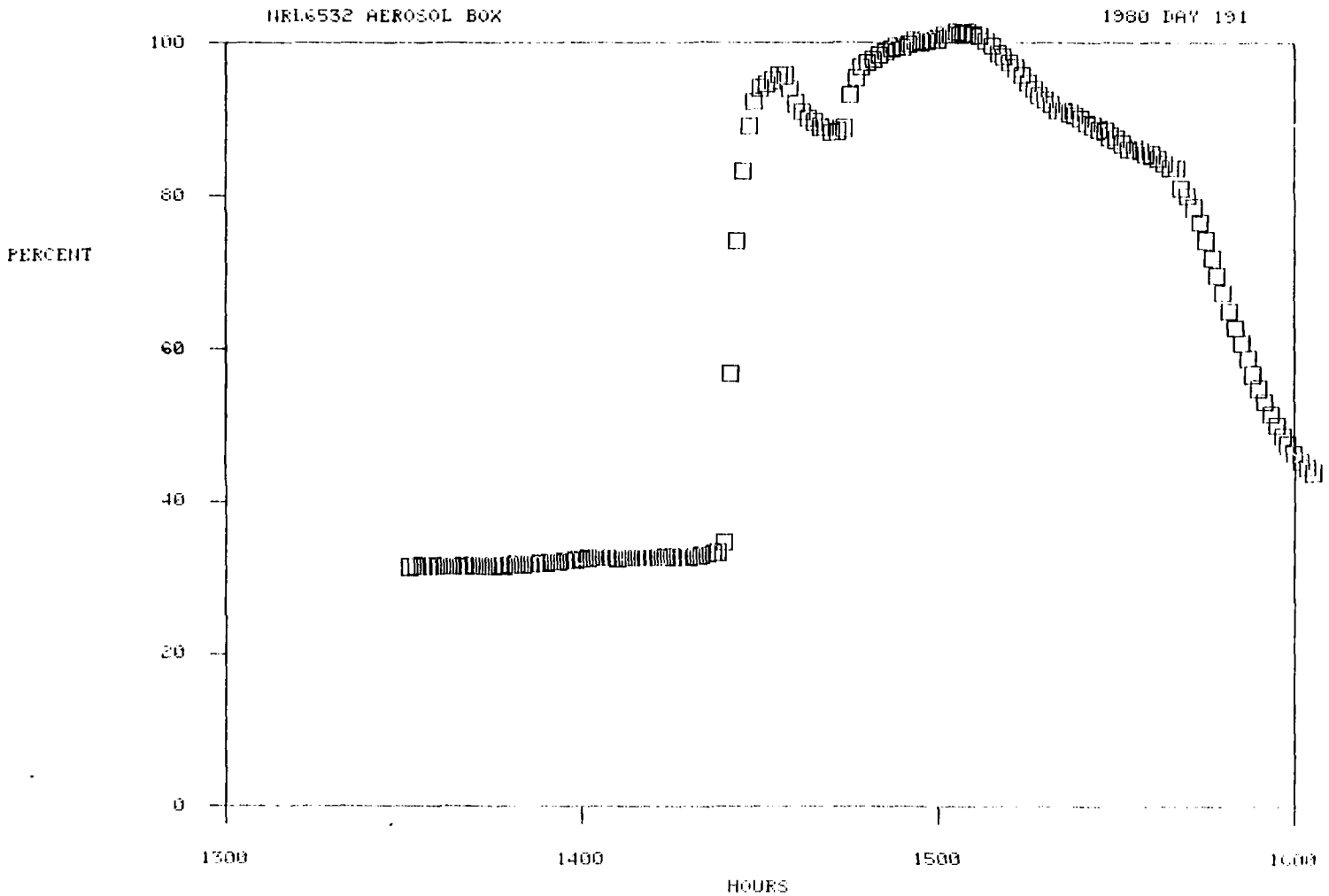

Fig. 6 — Relative humidity in the aerosol box as a function of time and generation

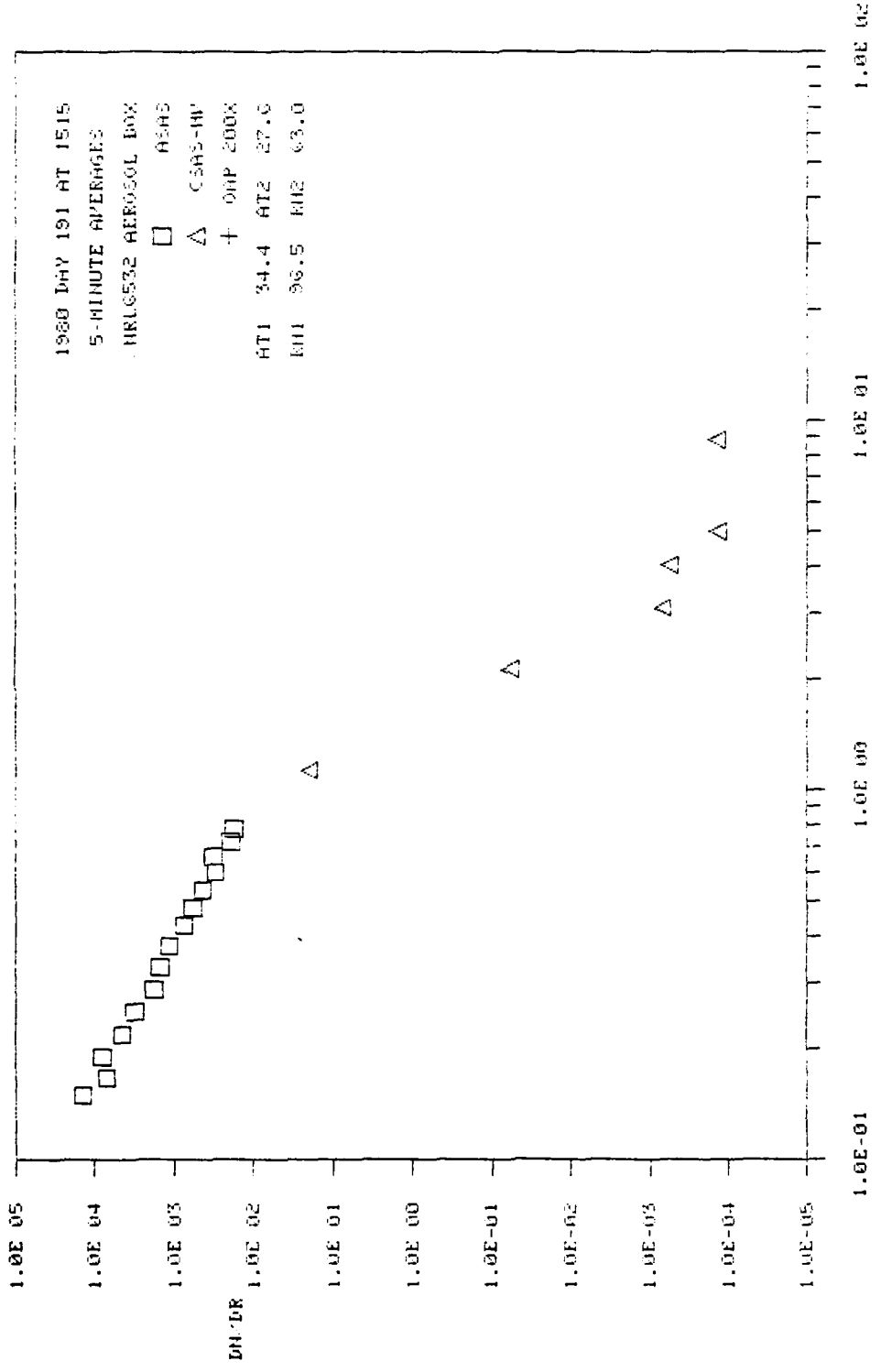

Fig. 7. — An aerosol-particle size distribution in the box after fog spray shut-off

A look at the time variation of the aerosol particle counts during this entire period is shown in Figs. 8 and 9. Figure 8 shows the particle count density for the particles counted by bin #1 of the CSASP-HV, i.e., the particles sized between 0.75 and 1.7 μm. These relatively small particles follow the relative humidity quite closely in the box for the described experiment. On the other hand, larger particles, as counted by bin #11, i.e., particles sized between 10.25 and 11.2 μm exist, effectively, only while generation occurs. They tend to fall out within a minute after the nozzles have shut off, as Fig. 9 demonstrates.

The conclusion for large-particle studies is, then, that a steady state condition with constant generation is required. We found, however, that after high relative humidity was attained the fog nozzles were not necessary for sustaining an increased-count aerosol-particle size distribution. The Ward's Cool Mist Vaporizers produced a different and therefore useful, size distribution, which we made use of during the breakdown experiment. They also produced much less liquid to have to remove from the box.

THE EXPERIMENTAL AEROSOL DISTRIBUTION

We show in Fig. 10 two aerosol-particle size distributions from open-sea conditions which typify the marine aerosol. It is obvious that Fig. 5 does not reproduce this marine aerosol—there are several orders of magnitude more particles in all size ranges in the generated distributions. This overkill is required, however, for statistical reasons. In the marine aerosol there are very few particles larger than 5 μm. And, for a reasonably-sized laser, the laser beam cross-sectional area times the pathlength through the aerosol box, i.e., the atmospheric volume encountered by a propagating laser pulse, is a value so small that for the natural marine particle size distribution there is, on the average, less than one particle in the beam larger than 5 μm. Thus it is necessary to increase the total count well above the naturally occurring values if statistically meaningful data are to derive from the breakdown experiment.

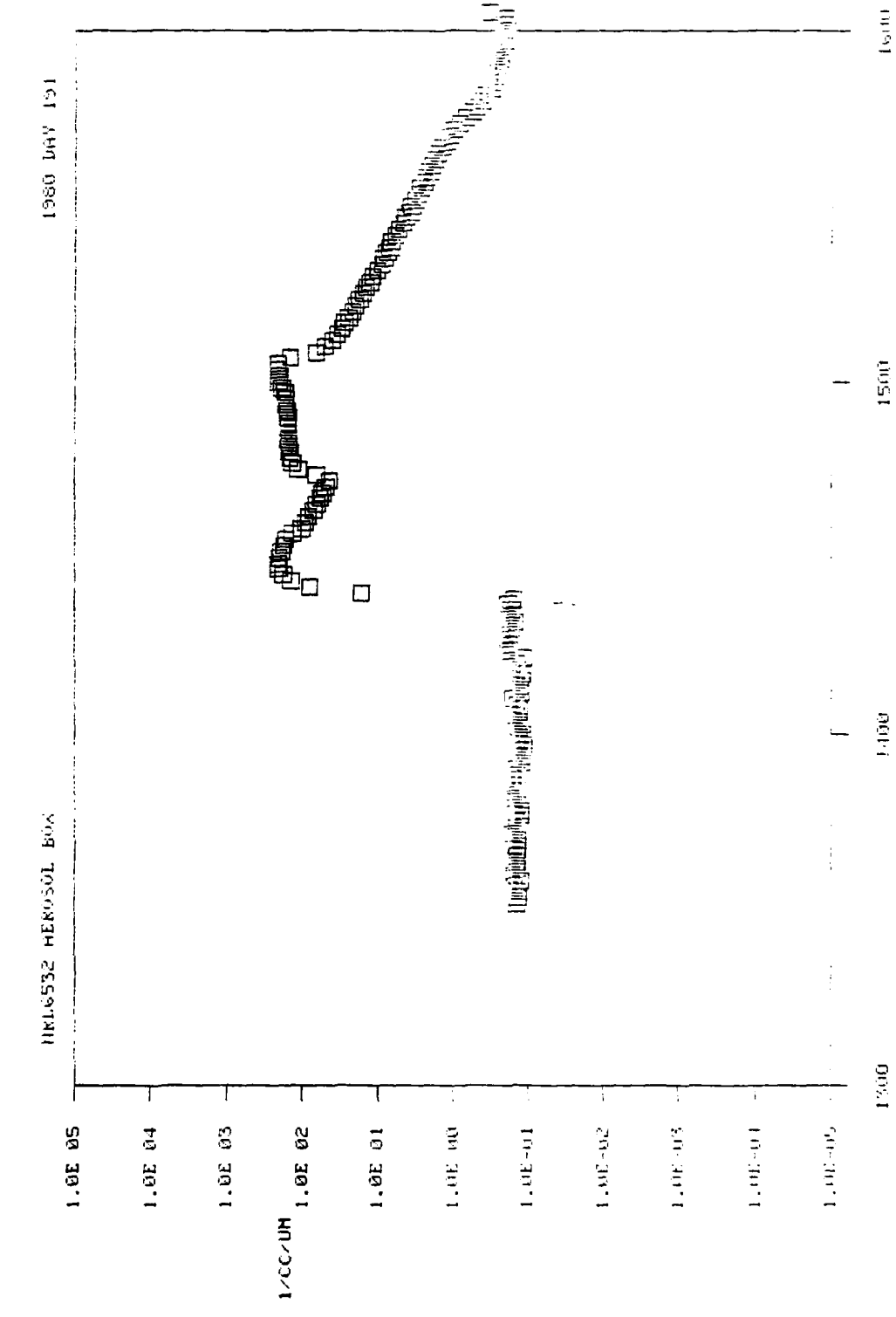

Fig. 8 — 1.1-μm particles as a function of time and generation

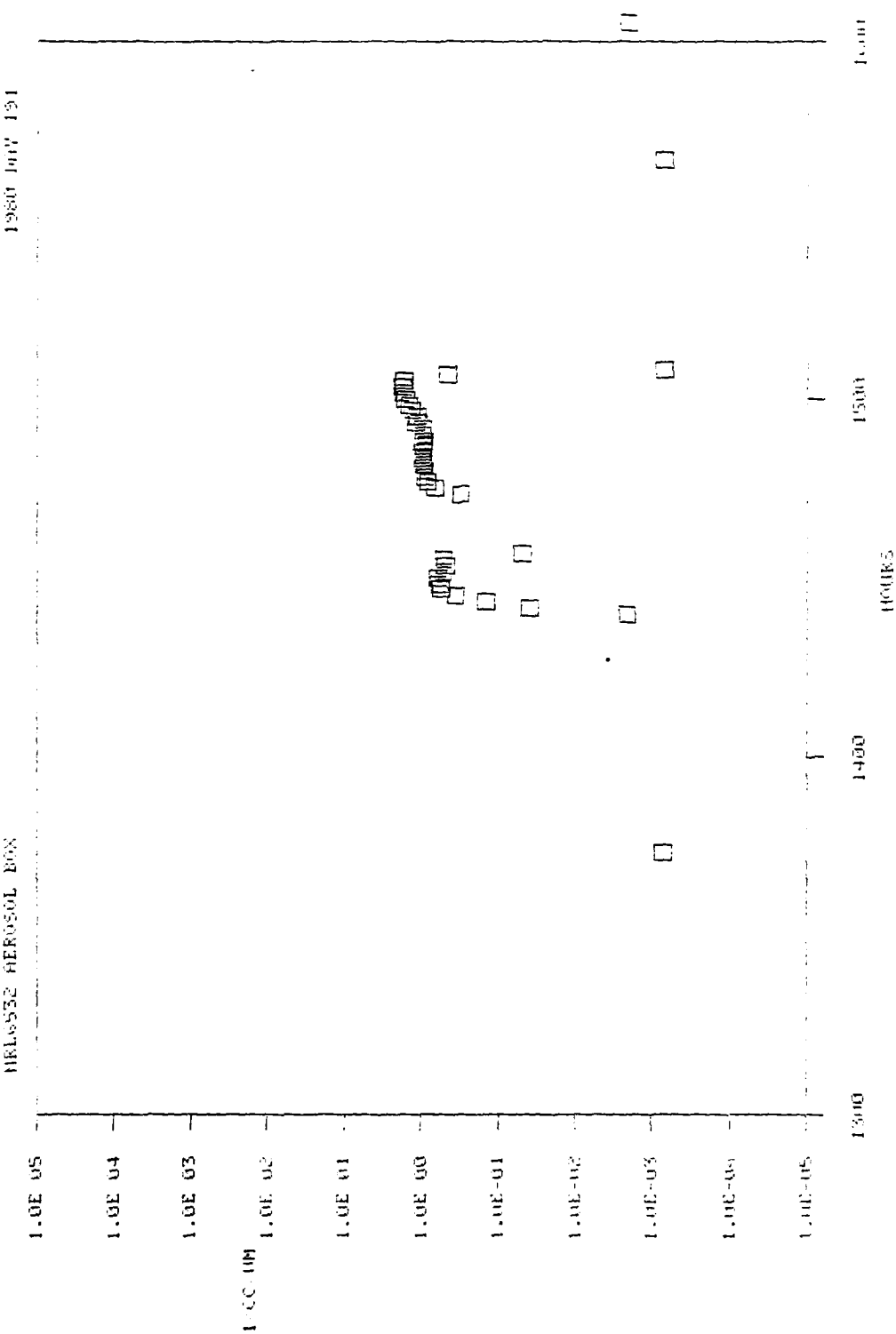

Fig. 9 — 11-μm particles as a functional time and generation

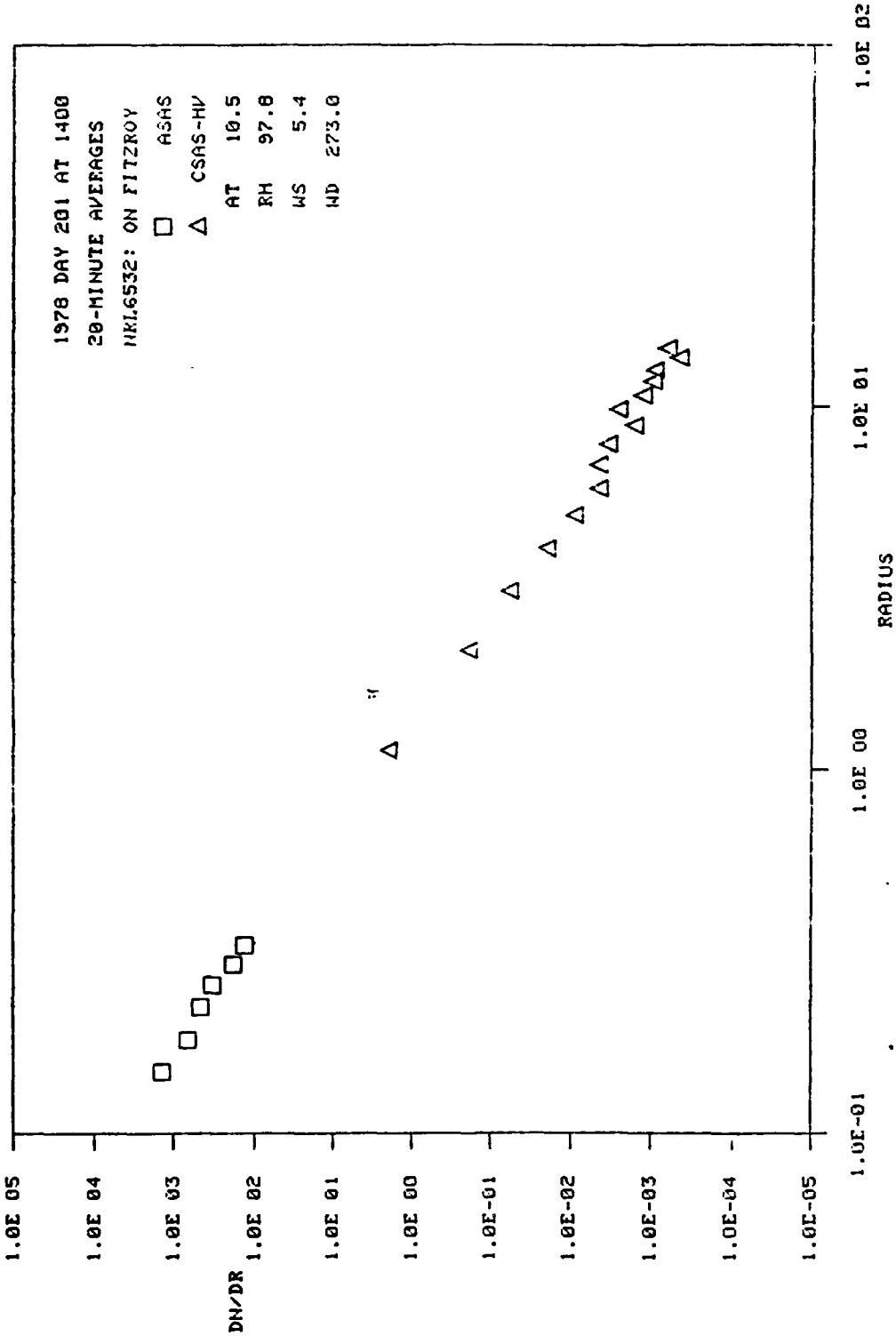

Fig. 10a — An aerosol-particle size distribution measured in the Mid-Atlantic

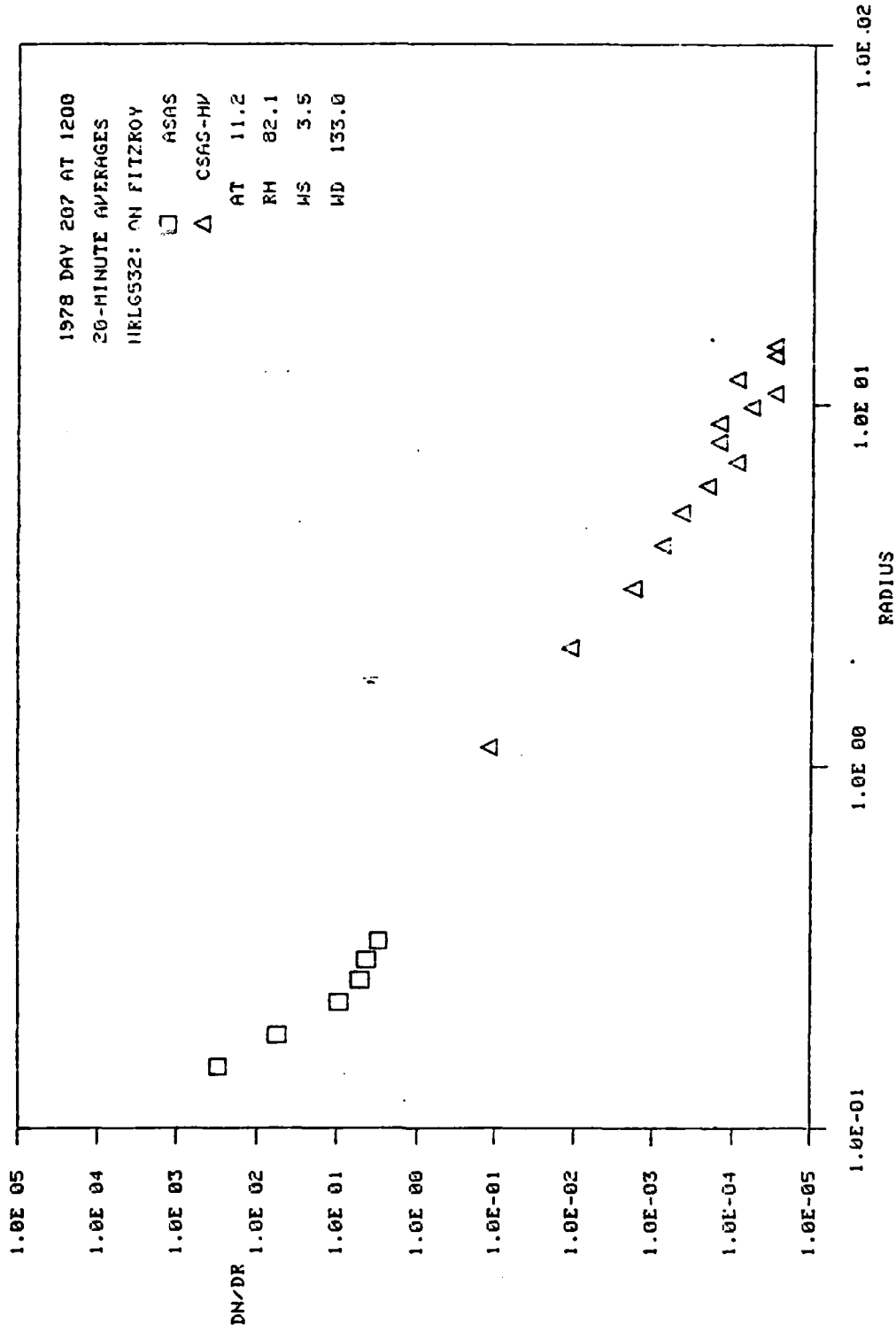

Fig. 10b — Another open-sea aerosol-particle size distribution measured in the Mid-Atlantic

A second determining factor is laser power density. The beam from Aerospace laboratory-size laser was necessarily focused to a small cross-section in order to reach sufficient power density for breakdown, which, of course, reduced the total beam volume. For example, during the tests at Aerospace, for a collimated beam of 0.6 cm diameter the volume of the beam through the aerosol region was about 100 cm^3. With the power available this gave approximately 28 MW/cm^2, and breakdown did not occur at this power density for our generated aerosol. Either the power was below threshold or there were no large breakdown-causing particles in the beam—or both.

It was necessary, therefore, to focus the beam to attain a sufficient power density for breakdown. Although this reduced the number of exposed aerosol particles, breakdown did occur. And, Fig. 11 shows the aerosol-particle size distribution at the time of the first successful breakdown shot, which in this case occurred at over 100 MW/cm^2.

Before discussing the distributions with respect to breakdown, note that there is an extra curve in Fig. 11. This experiment required that we be able to readily obtain the density of particles $N(R)$ larger than a given size, R. The usual dN/dR curve does not give that, but must be integrated to give

$$N(R) = \int_R^\infty \frac{dN}{dR'}\, dR'.$$

The advantage of having an on-board computer is that simple changes in the data display are readily rendered on-site. We did just that at Aerospace and the result is given by the diamonds in Fig. 11 and in all the size distribution plots that follow.

We are including here in Figs. 11 through 29, all the aerosol-particle size distributions obtained during and after the first breakdown shot, i.e., one for each successful shot into the box. Each figure caption contains the Aerospace-assigned number of that particular laser shot. Missing shot numbers imply beam diagnostic firings (such as alignment checks) or misfirings.

The curves of $N > R$ versus R appear to have discontinuities where the results of two different probes meet. This is an artifact of two processes. In the measurement the probes are not efficient at

the smallest ranges. In the post-measurement integration, which is done in the histogram manner, a discontinuity appears where there is a large change in bin size. Also, for the ASASP (.13-.75 μm), the six largest bins often over-count due to a double valued sensitivity function near particle sizes about the wavelength of the HeNe laser used in the measurement process. Correct interpretation, then, requires some smoothing of the data near the points where the probe ranges join.

The discontinuities in the mid-ranges of the two large-particle probes, however, are likely to be real, indicating a multimode particle-size spectrum resulting from selective generation by the particle generators. Figures 13 through 16 (as well as others), for example, show a particularly strong break near 3.5 μm.

In Figs. 20 through 24 the fog nozzles had obviously been shut off sometime prior to firing. Also included there are three shots where the dew point device malfunctioned.

Table I gives a summary of the shots fired with a few notes. Except for the last two shots all particle generation was done with distilled water. As a check on fresh-water-versus-salt-water effects we put sea water in the spinning-disc generators. We saved this experiment for the end to avoid possibly destroying the generators early in the experiment. The column marked "DF Laser Fill" indicates laser cavity gas pressure at the time of firing, giving a rough relative value for energy in the pulse.

BREAKDOWN DISCUSSION

In order to achieve breakdown it was necessary to focus the beam to a rather small spot, the volume where breakdown occurred being less than 1 cm^3. Unfortunately, this means that, on the average, very few particles of any appreciable size are exposed to the beam. Reading from Fig. 11, e.g., we would not expect to find any particles larger than about 20 μm in that 1 cm^3 space. And, to be safe statistically, we might prefer to have ten particles, which translates to less than ten particles larger than 8 μm. Similar readings can be taken from the other distributions. Clearly, a laser pulse energy ten times greater would enable a ten times larger volume to be investigated.

At the time of this writing the calibrated volumes for the laser firings were not available, so detailed discussions are not appropriate. Details of the 3.8 μm breakdown threshold intensity vs particle size distribution, and pulse length, will be contained in a future publication after these laser parameters become available. It is obvious, however, that to do this experiment properly a laser with much higher output power should be used, preferably larger by at least a factor of ten.

PLANS

Before returning to a laser site, we would do further testing of aerosol generation in the chamber to learn the best technique for obtaining the desired assortment of particle spectra. One such experiment will involve burning a small measured amount of a pyrotechnic which produces hydrophilic particles. Although the particles from this technique are initially small, a high-humidity condition in the chamber would soon produce the desired large particles.

After testing this procedure the aerosol breakdown chamber and the data acquisition electronics would both again be transported to the site for the experiment.

ACKNOWLEDGMENT

The authors wish to thank K. Winters and B. Eckert for the typing of this report and C. Acton for his excellent photographic work. F. Tidball and P. Delaney assisted in fabrication of the aerosol chamber.

This work was sponsored by the Pulsed Chemical Laser program.

REFERENCES

1. D.C. Smith, "Laser-Induced Gas Breakdown and Plasma Shielding," SPIE Proceedings, Vol. 195. (Atmospheric Effects on Radiative Transfer), 1979, 171-181.

2. D.E. Lencioni, "The Effect of Dust on 10.6 μm Laser-Induced Air Breakdown," Appl. Phys. Lett., 23, 12 (1973).

3. G.L. Trusty and T.H. Cosden, "Optical Extinction Predictions from Measurements on the Open Sea," NRL Report 8260, Naval Research Laboratory, Washington, D.C. 20375, (January 19, 1979).

4. G.L. Trusty and T.H. Cosden, "Optical Extinction Predictions from Measurements aboard a British Weather Ship," NRL Report 8497, Naval Research Laboratory, Washington, D.C. 20375, (August 27, 1981).

5. G.L. Trusty and K.M. Haught, "An Aerosol Data Base Format," NRL Memorandum Report 4065, Naval Research Laboratory, Washington, D.C. 20375, (September 24, 1981).

Table 1
A Summary of the Size-Distributions Obtained
During Laser Firings

Fig.	Shot #	Breakdown	DF-Laser Fill (Torr)	Aerosol
11	718	Yes		Fog Nozzles
12	719	Yes		Fog Nozzles
13	724	Yes	400	Fog Nozzles
14	726	Yes	300	Fog Nozzles
15	727	Yes	250	Fog Nozzles
16	728	No	200	Fog Nozzles
17	729	No	300	Filtered Air
18	731	Yes	300	Spinning Discs
19	732	Yes	250	Spinning Discs
20	733	No	250	Spinning Discs
21	734	Yes	400	Spinning Discs
22	735	Yes	325	Spinning Discs
23	736	Yes	280	Spinning Discs
24	737	Yes	280	Spinning Discs
25	738	Yes	220	Spinning Discs
26	739	Yes	225	Spinning Discs
27	740	No	200	Spinning Discs
28	741	No	200	Spinning Discs Salt Water
29	743	Yes	225	Spinning Discs Salt Water

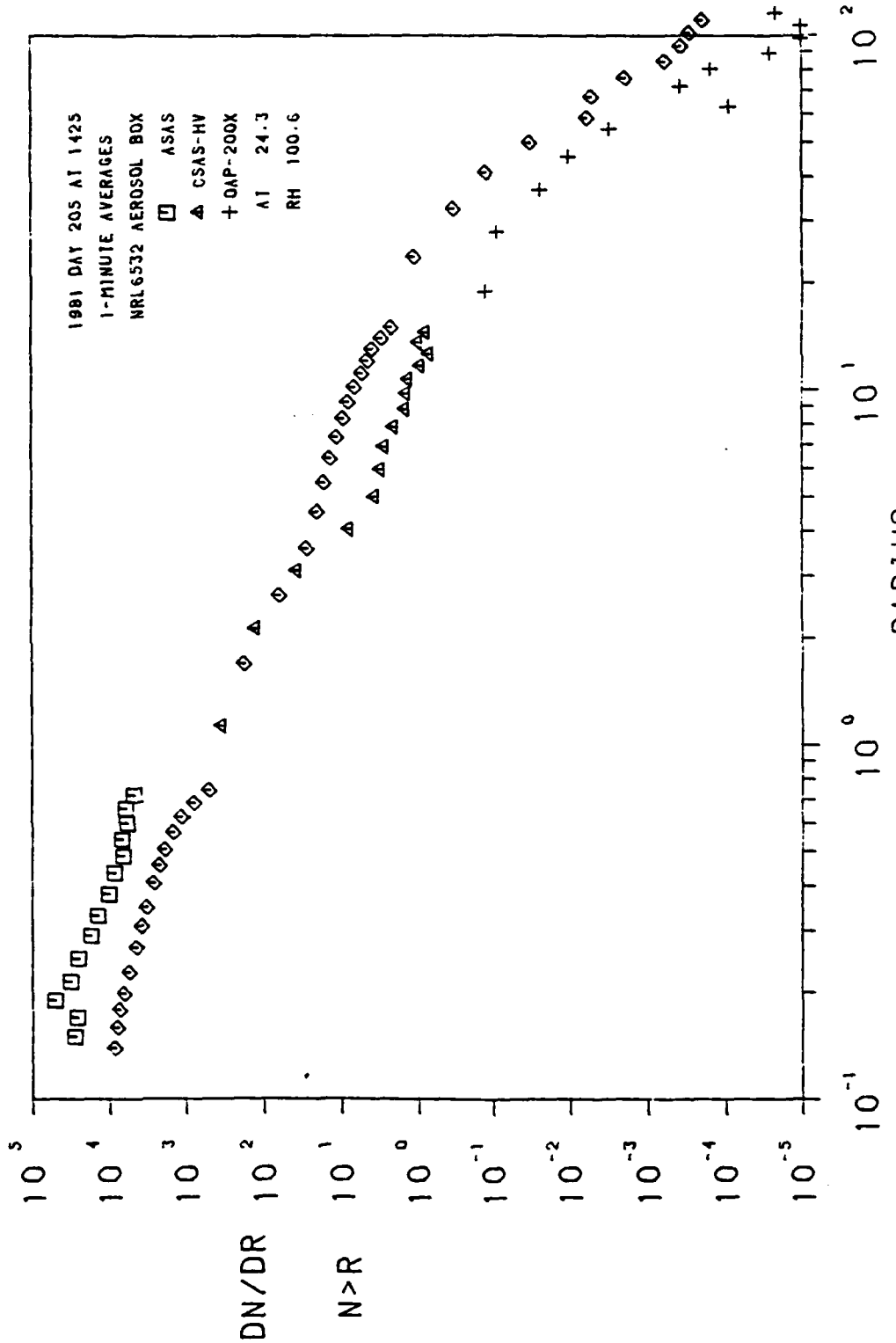

Fig. 11 – Particle size distribution for shot #718, breakdown

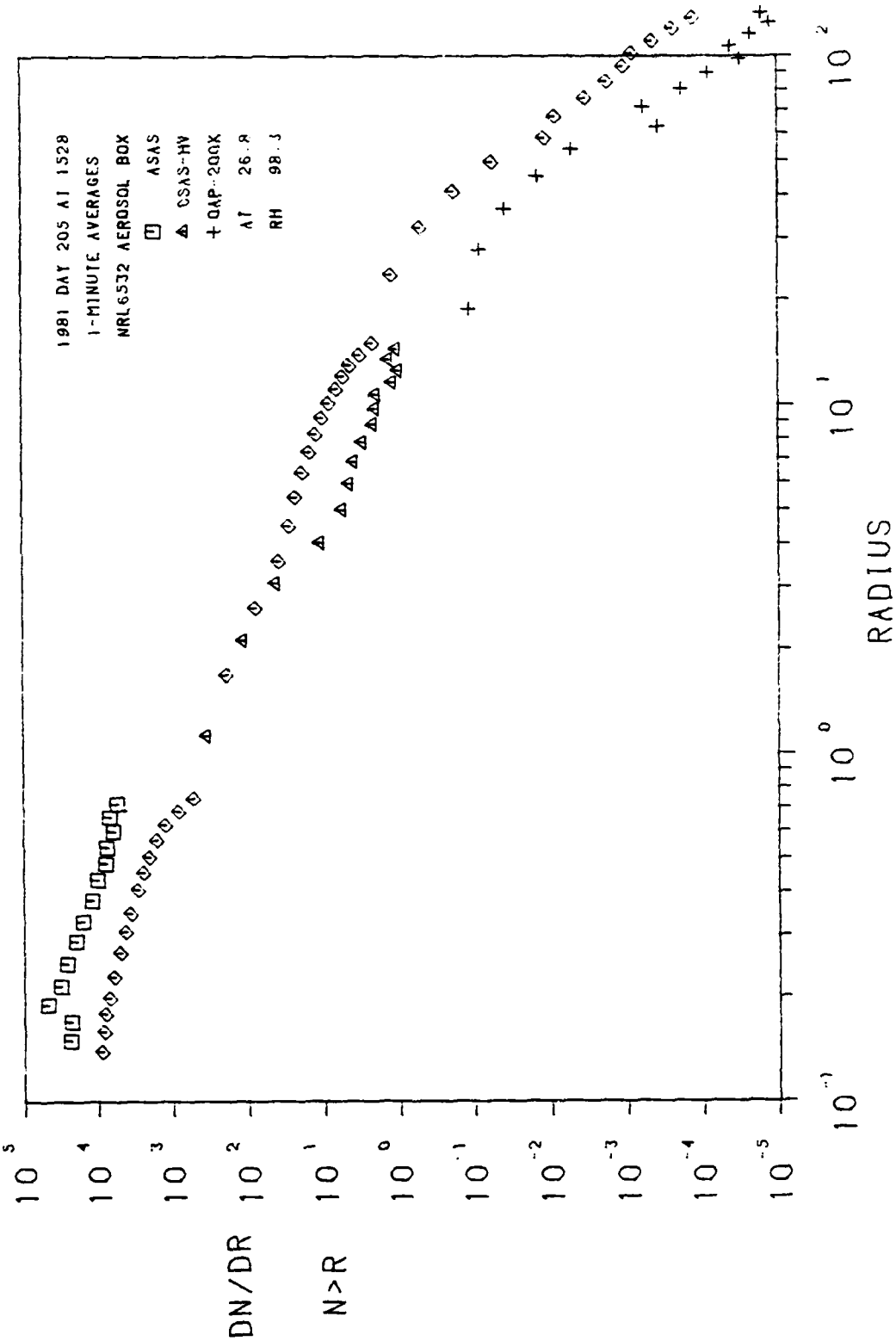

Fig. 12 – Particle size distribution for shot #719, breakdown

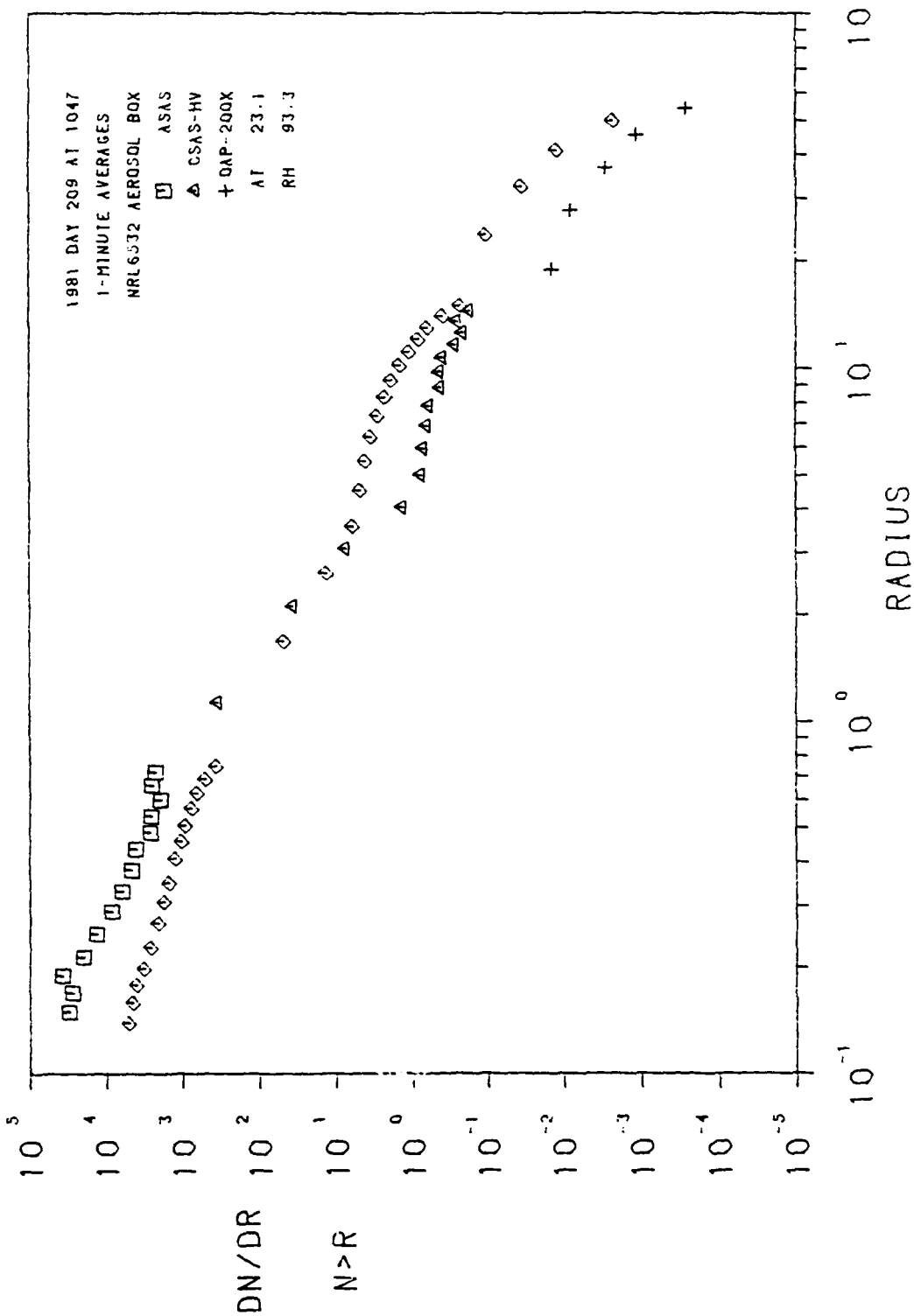

Fig. 13 — Particle size distribution for shot #724, breakdown, 400 torr

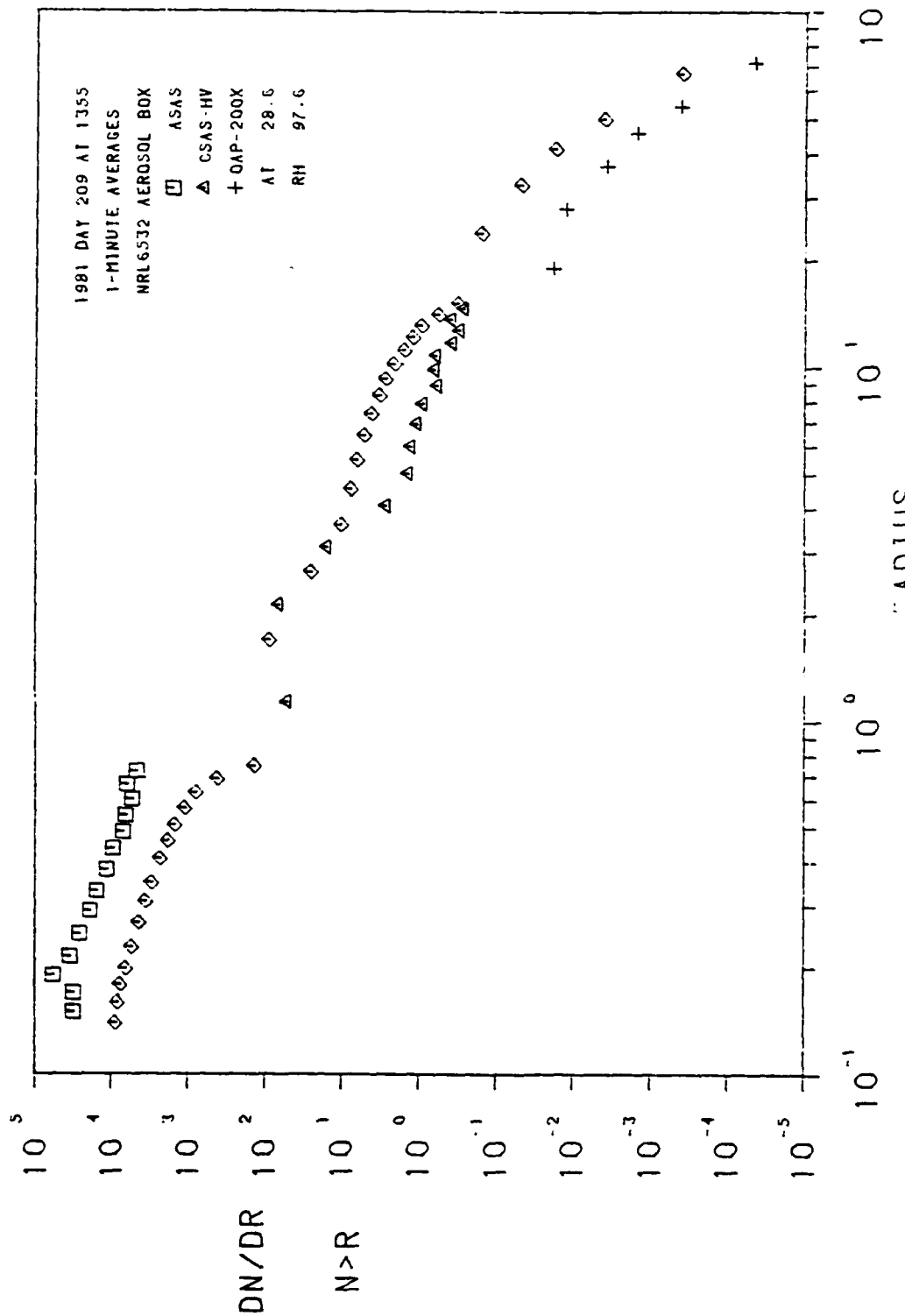

Fig. 14 — Particle size distribution for shot #726, breakdown, 300 torr

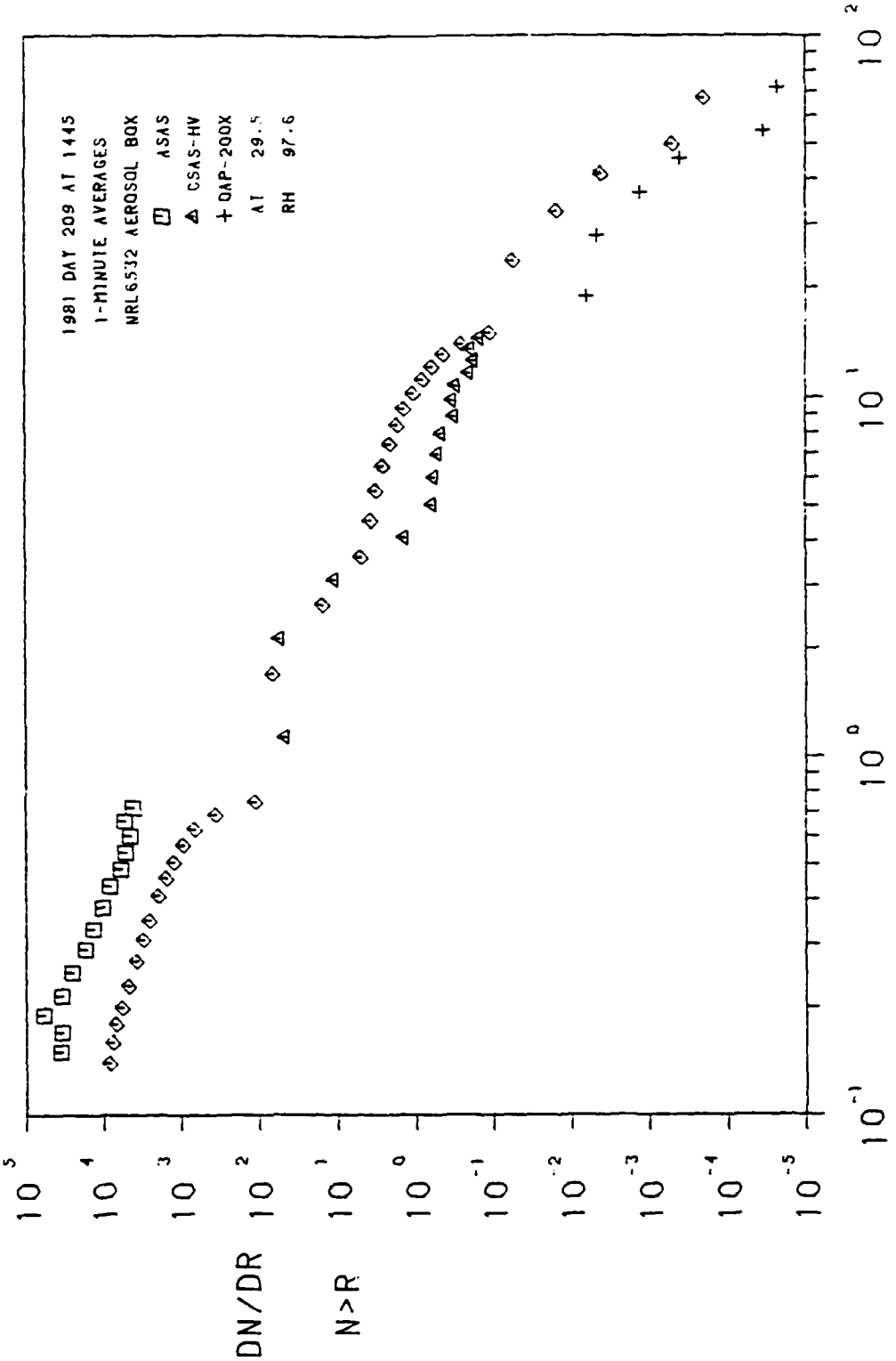

Fig. 15 — Particle size distribution for shot #727, breakdown, 250 torr

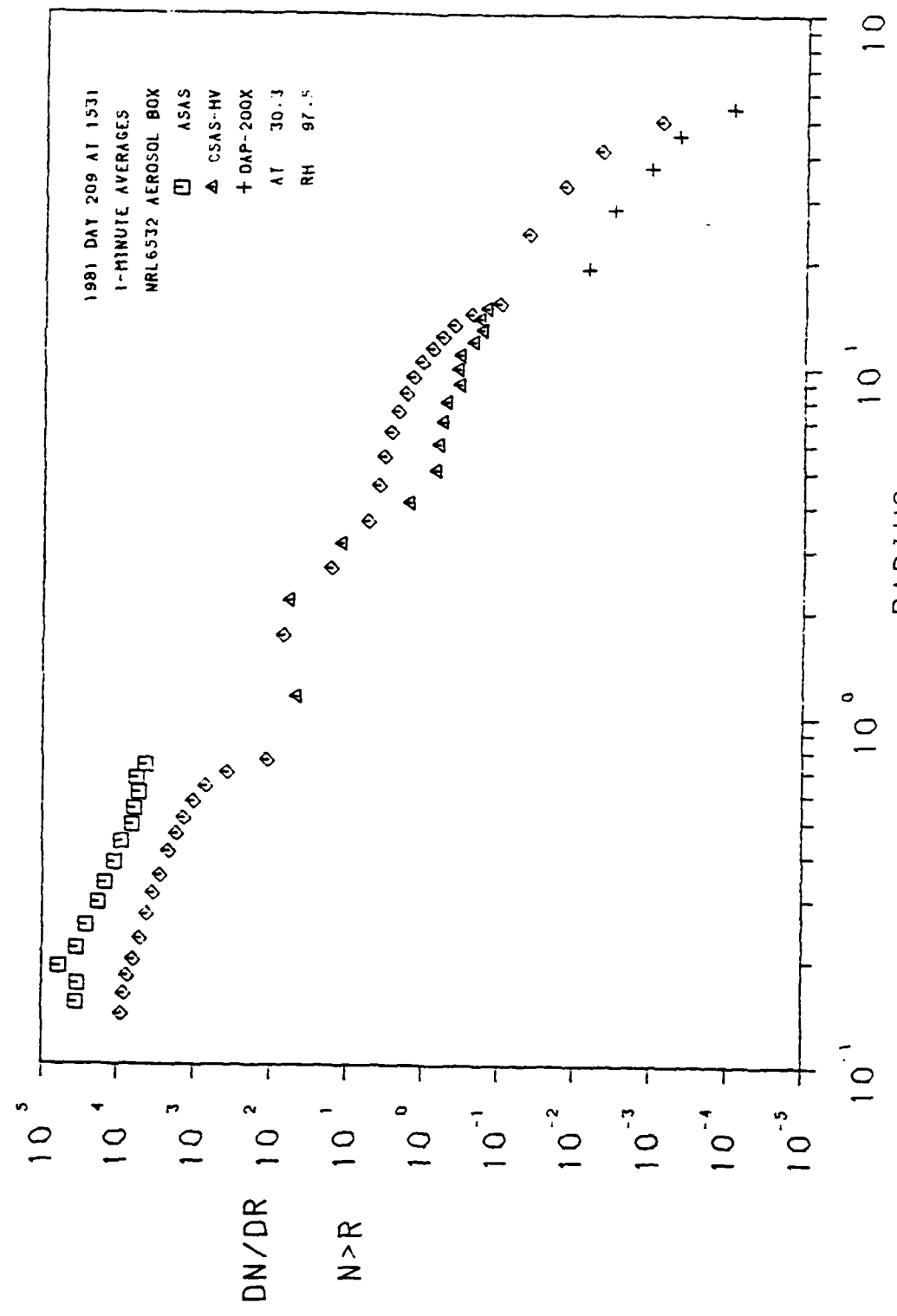

Fig. 16 — Particle size distribution for shot #728, no breakdown, 200 torr

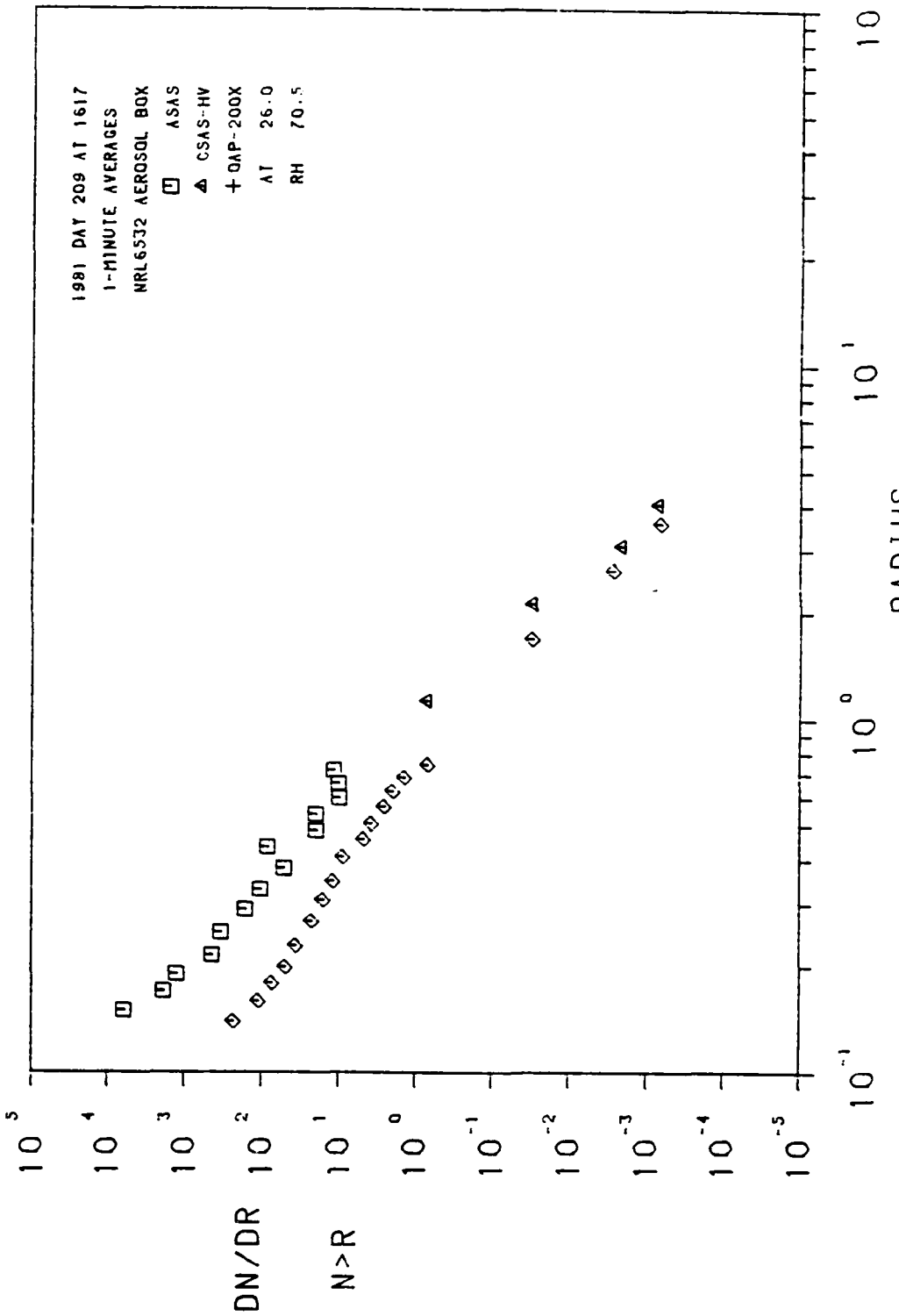

Fig. 17 — Particle size distribution for shot #729, no breakdown, 300 torr

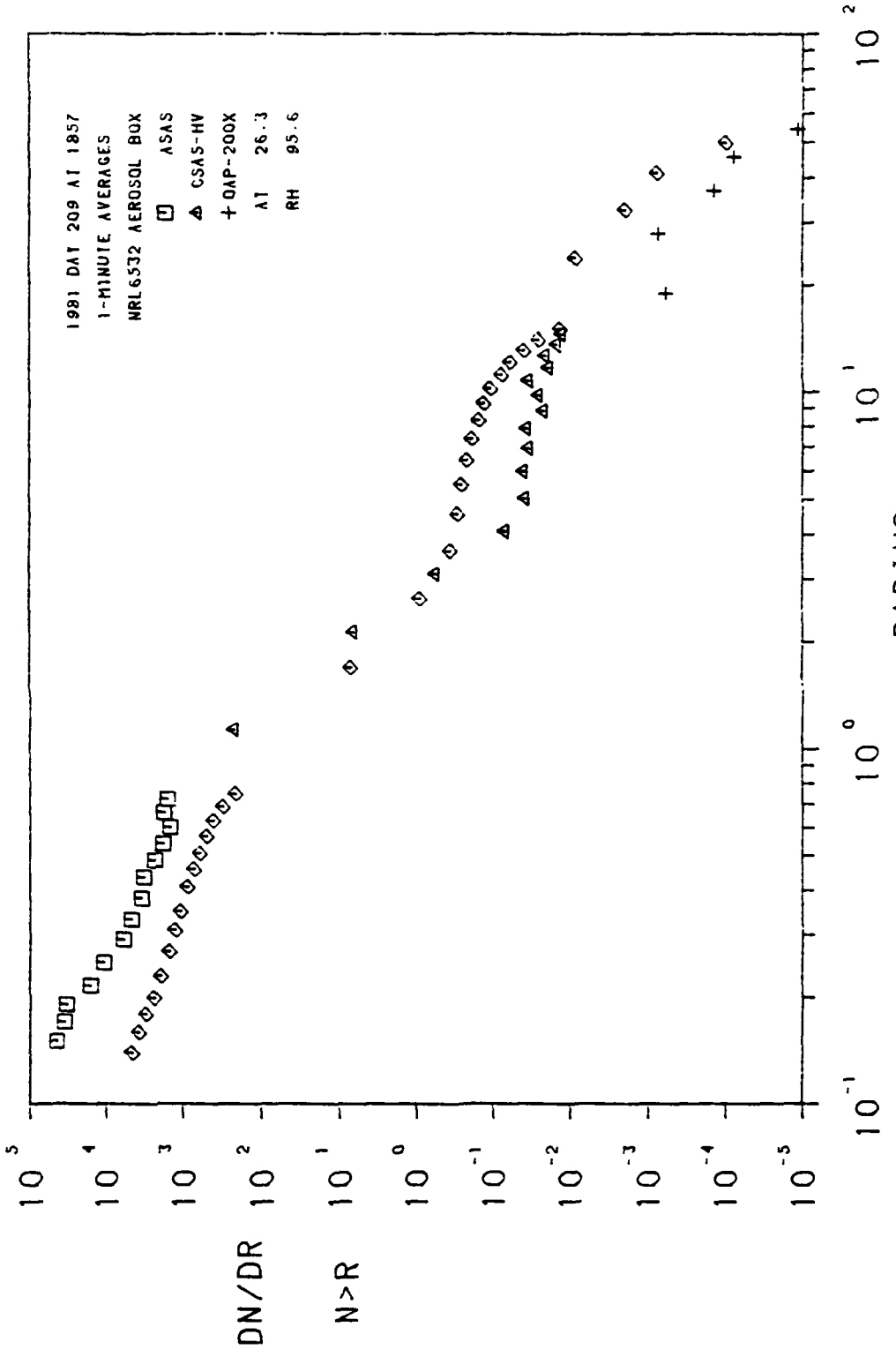

Fig 18 — Particle size distribution for shot #731, breakdown, 300 torr

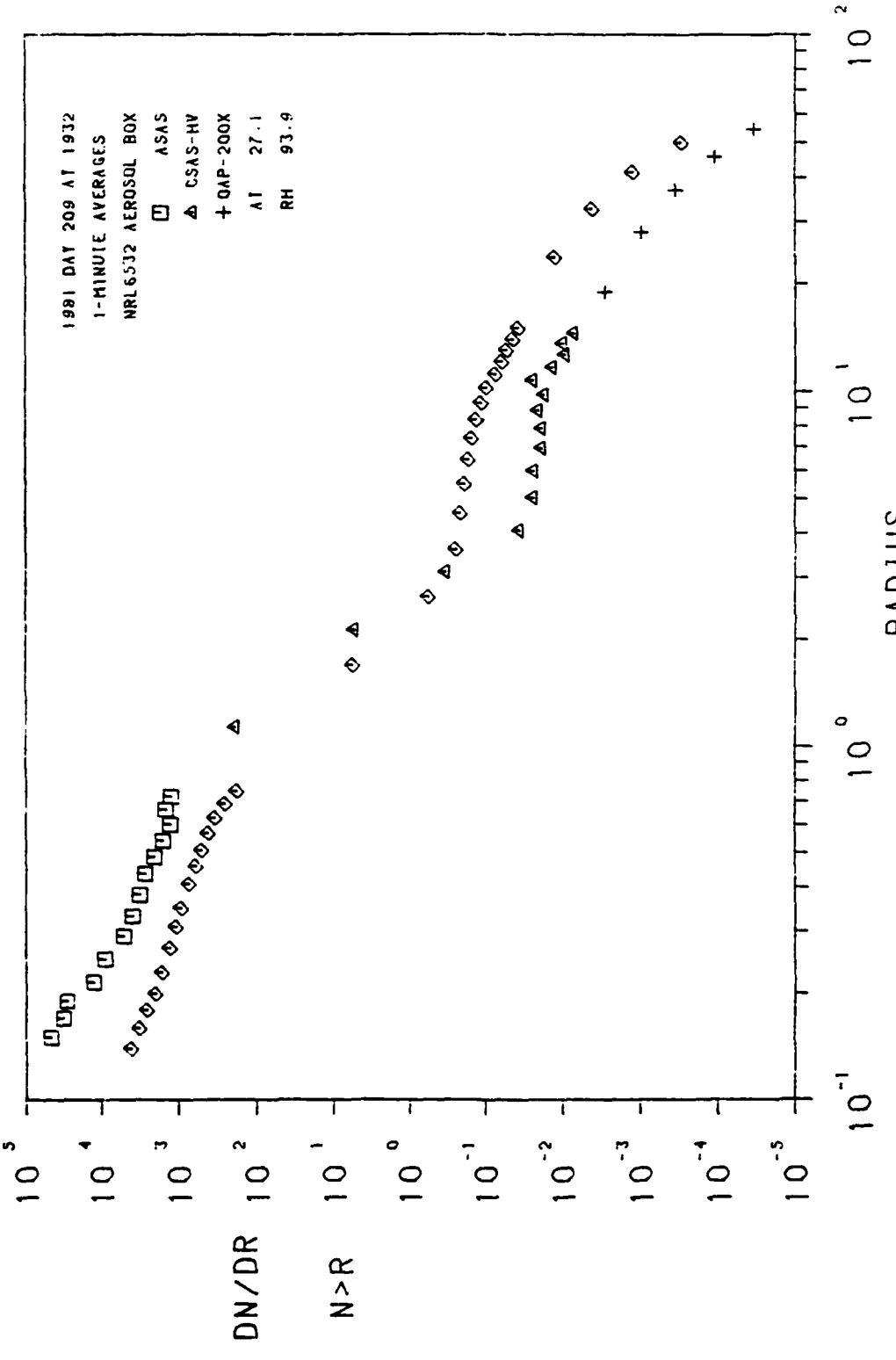

Fig. 19 — Particle size distribution for shot #732, breakdown, 250 torr

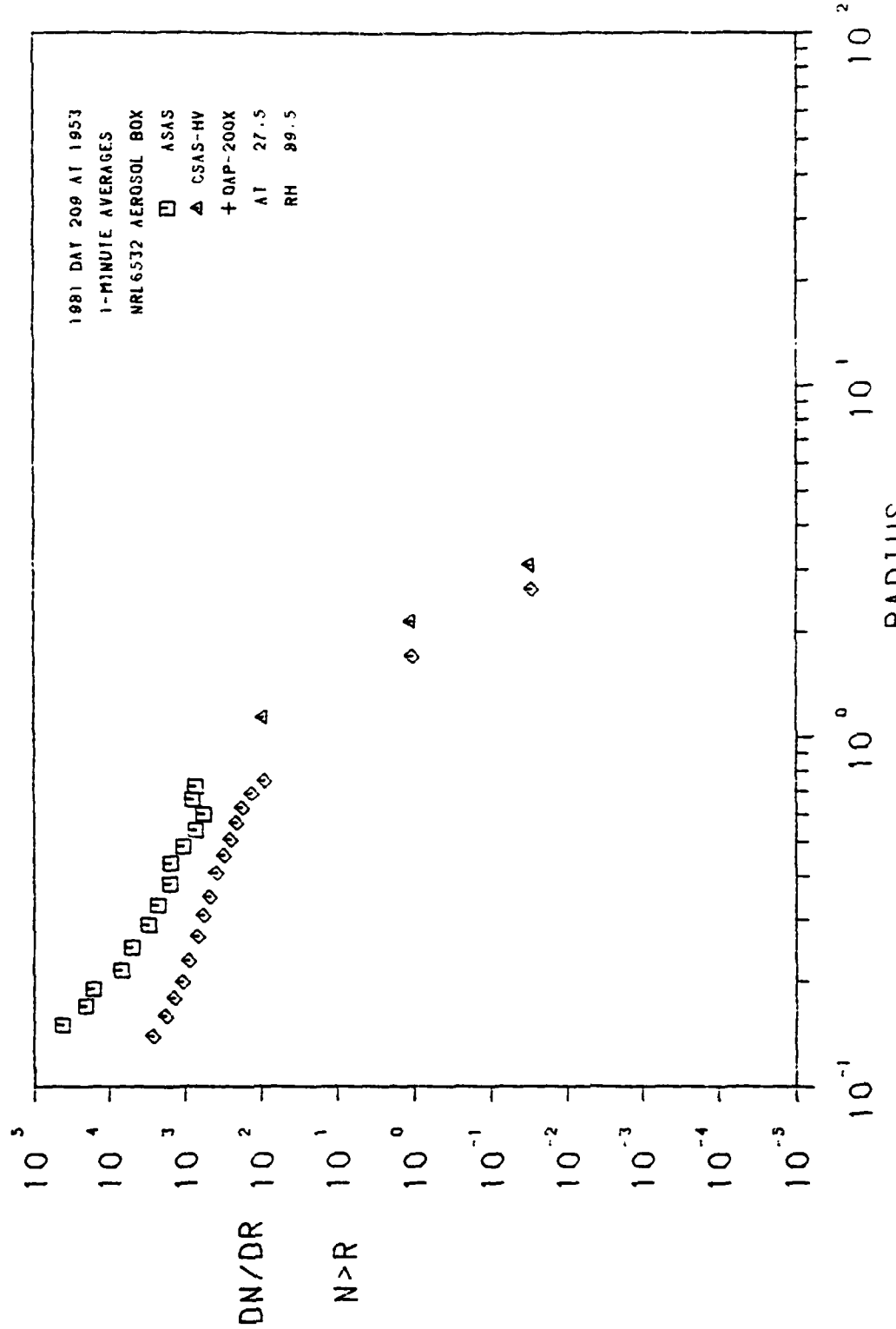

Fig. 20 — Particle size distribution for shot #733, no breakdown, 250 torr

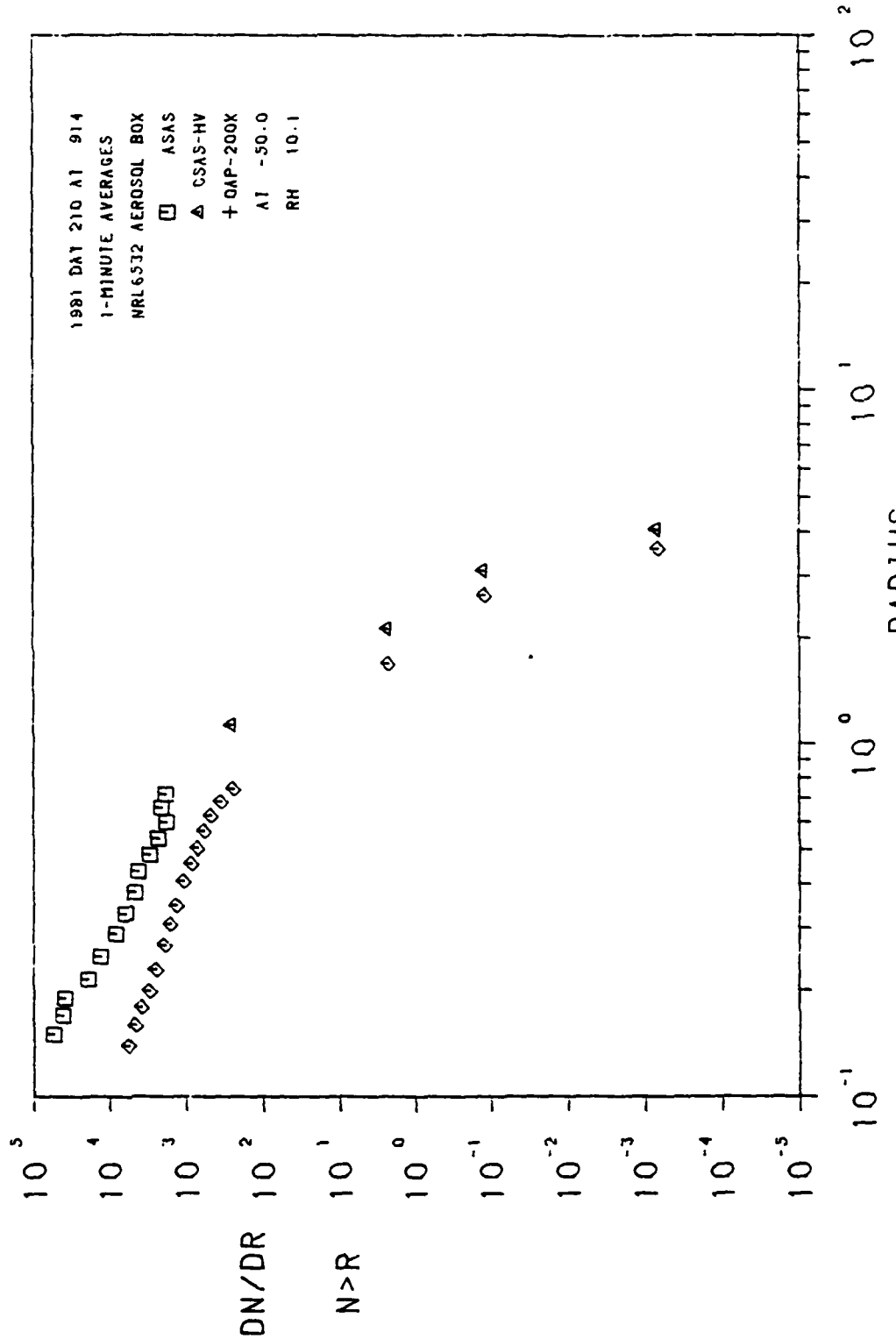

Fig. 21 — Particle size distribution for shot #734, breakdown, 400 torr

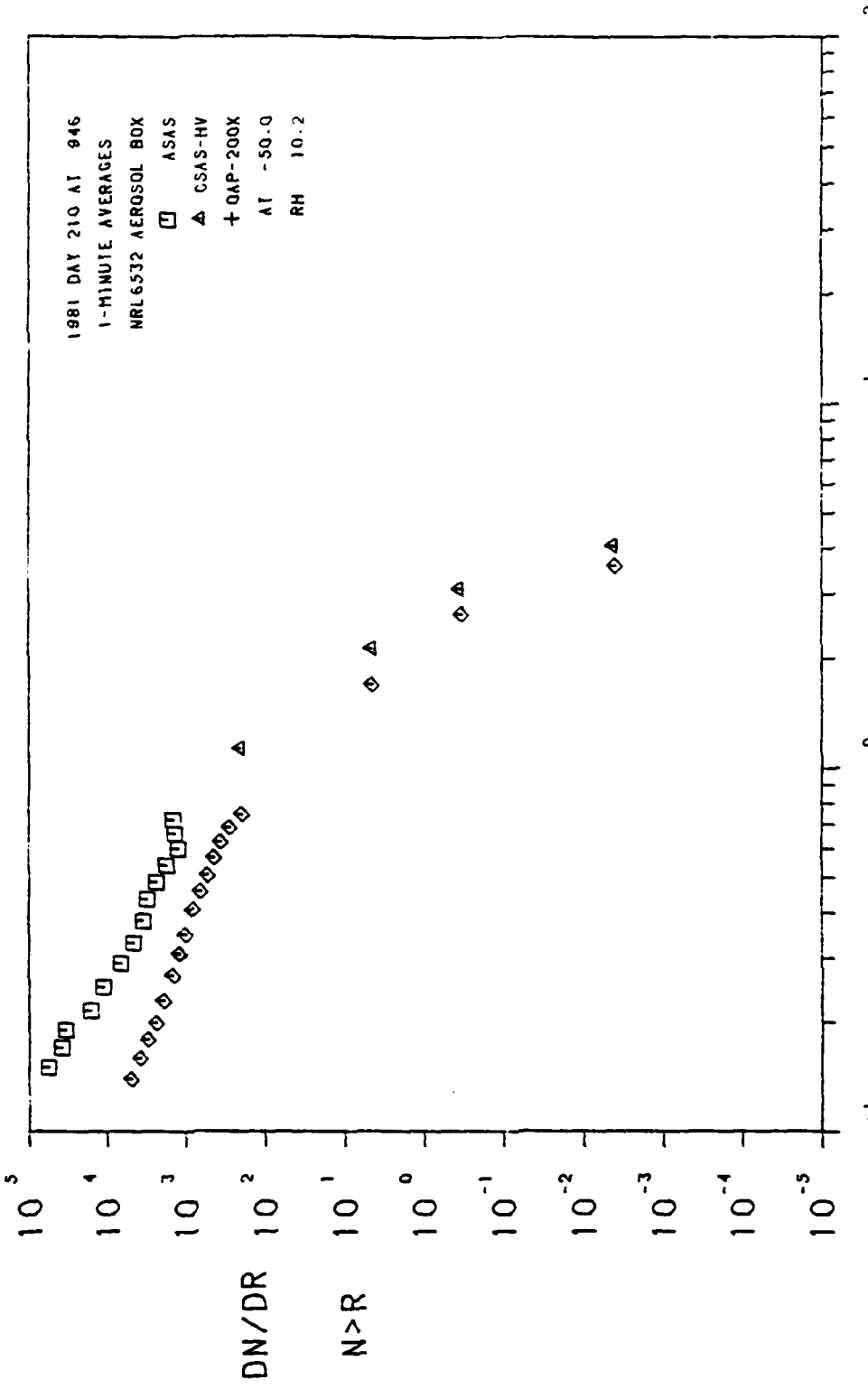

Fig. 22 – Particle size distribution for shot #735, breakdown, 325 torr

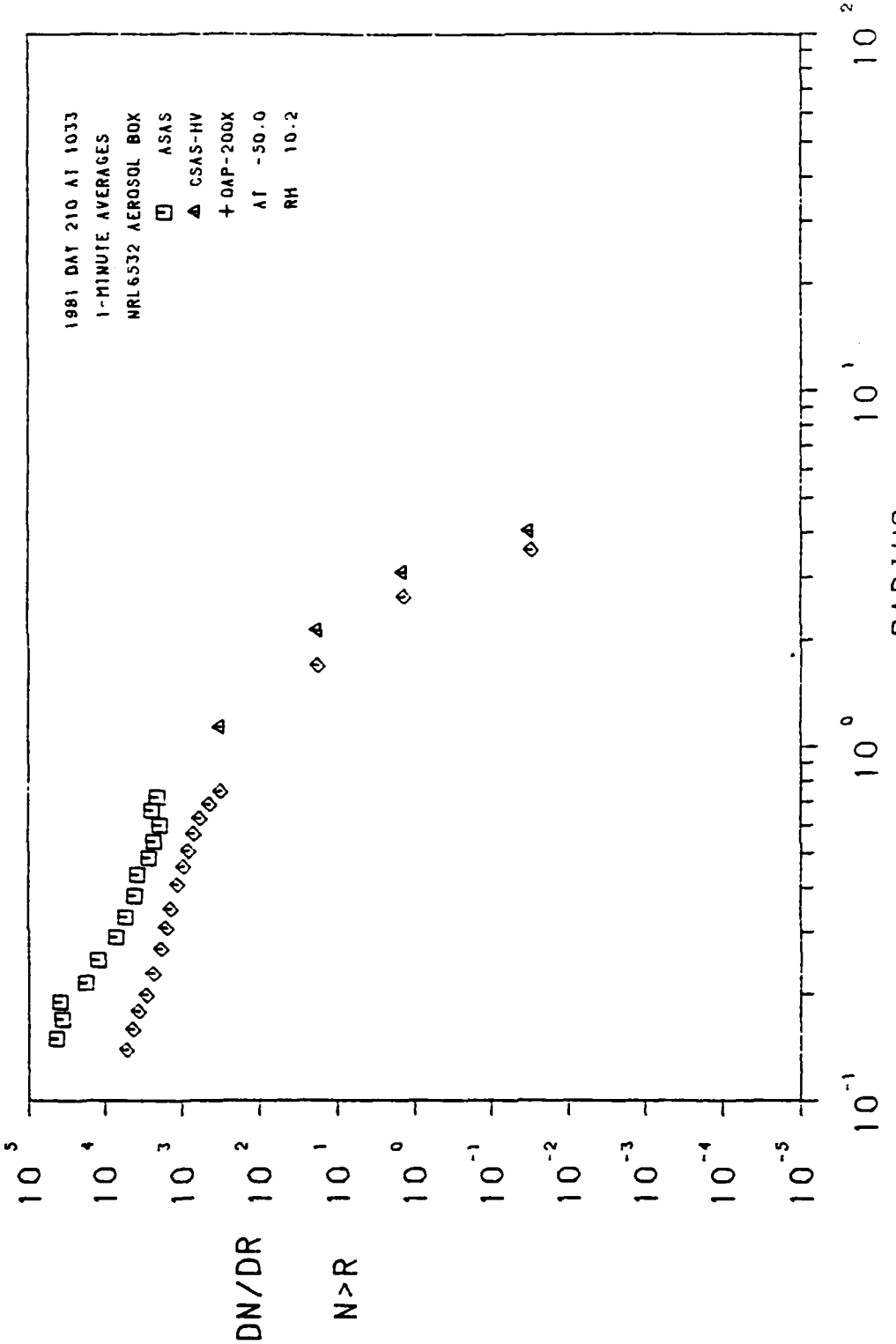

Fig. 23 — Particle size distribution for shot #736, breakdown, 280 torr

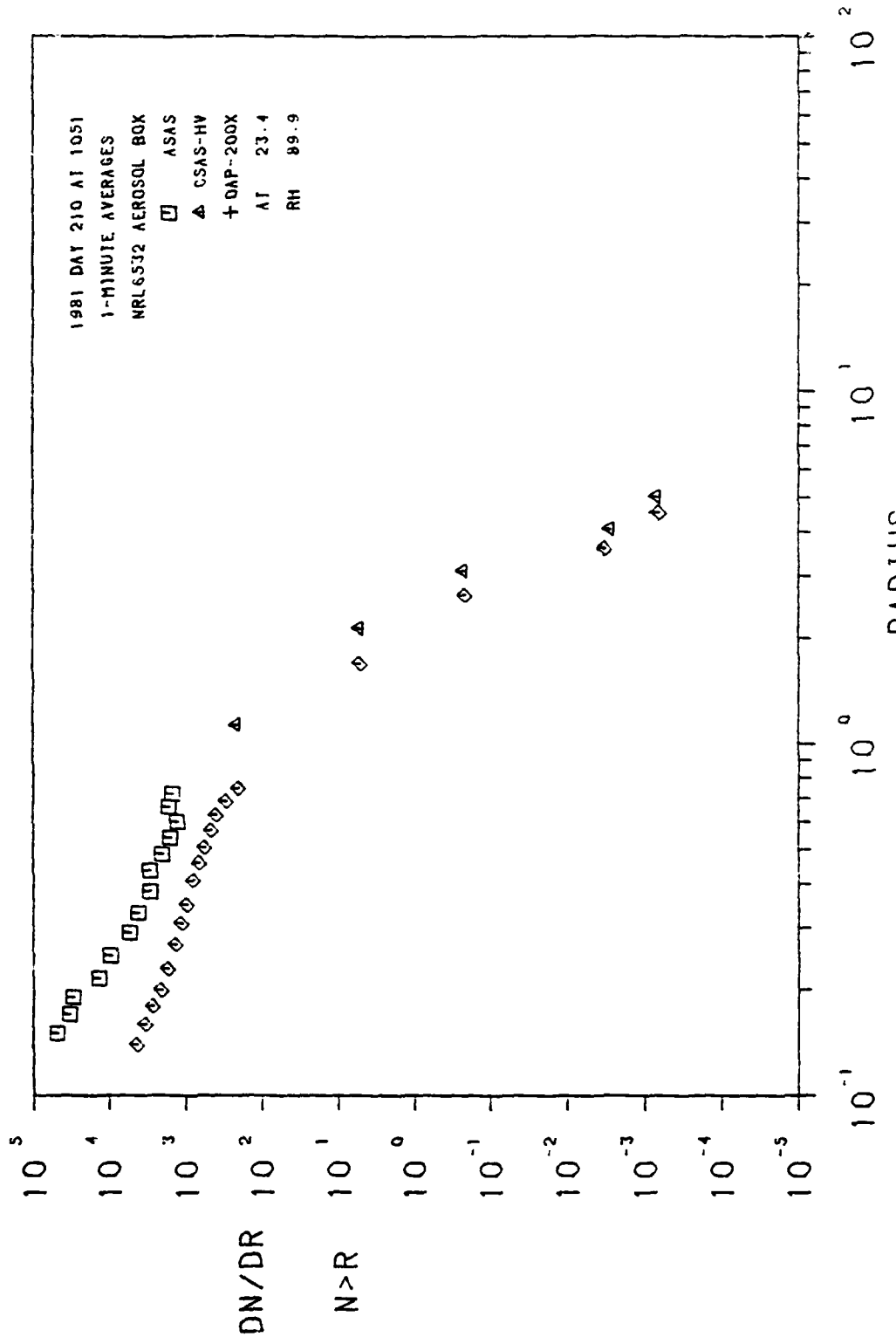

Fig. 24 — Particle size distribution for shot #737, breakdown, 280 torr

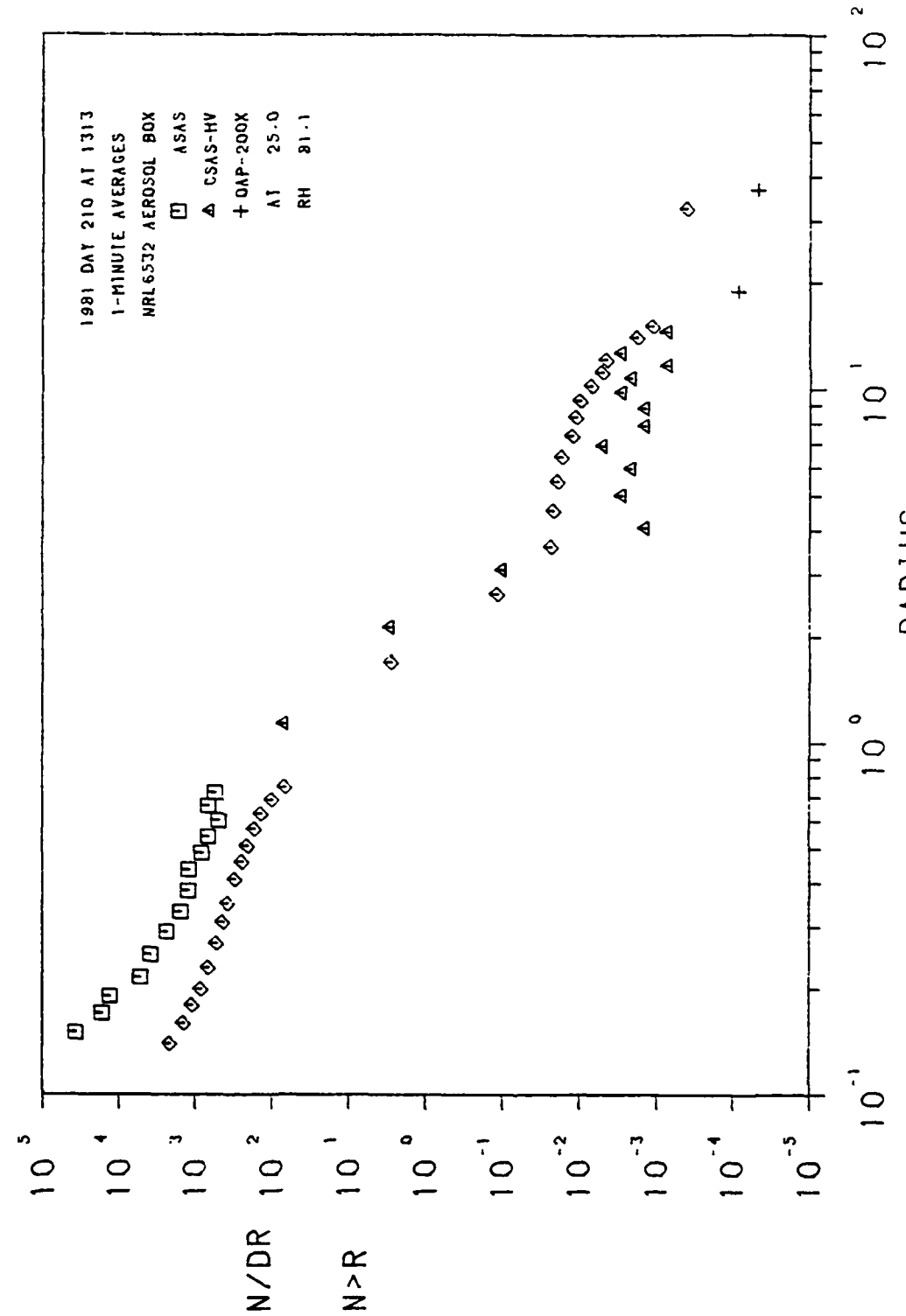

Fig. 25 — Particle size distribution for shot #738, breakdown, 220 torr

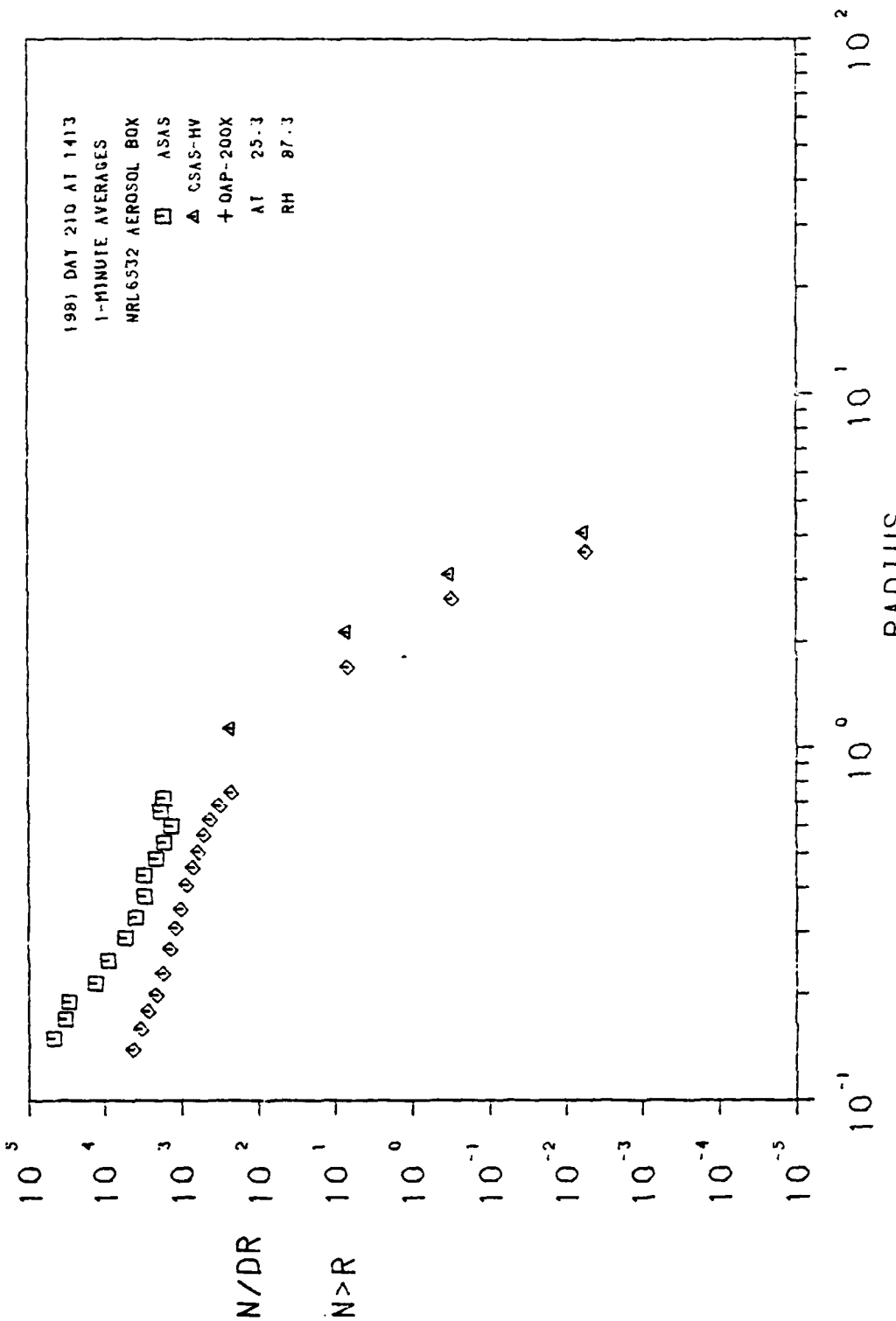

Fig. 26 — Particle size distribution for shot #739, breakdown, 225 torr

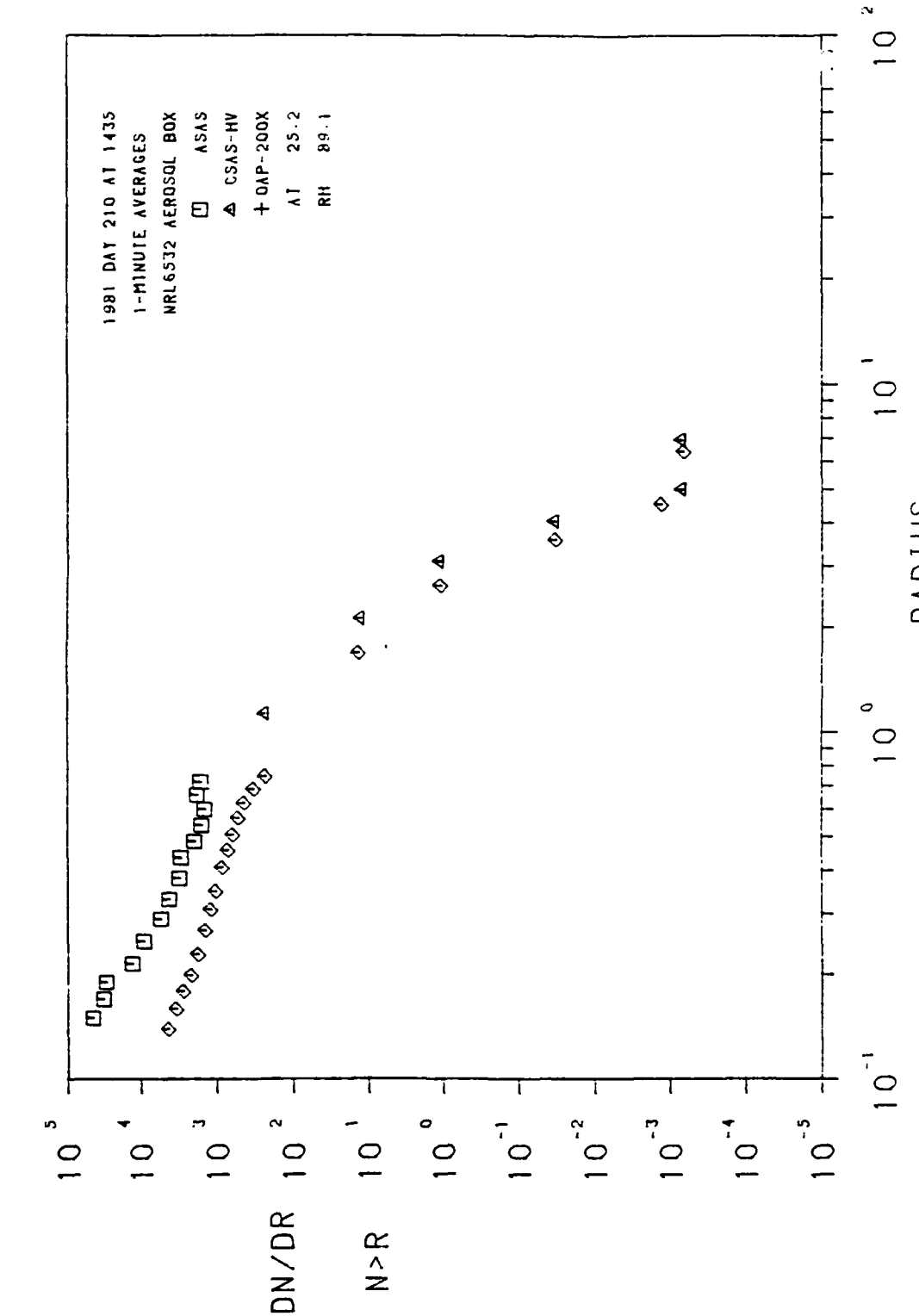

Fig. 27 — Particle size distribution for shot #740, no breakdown, 200 torr

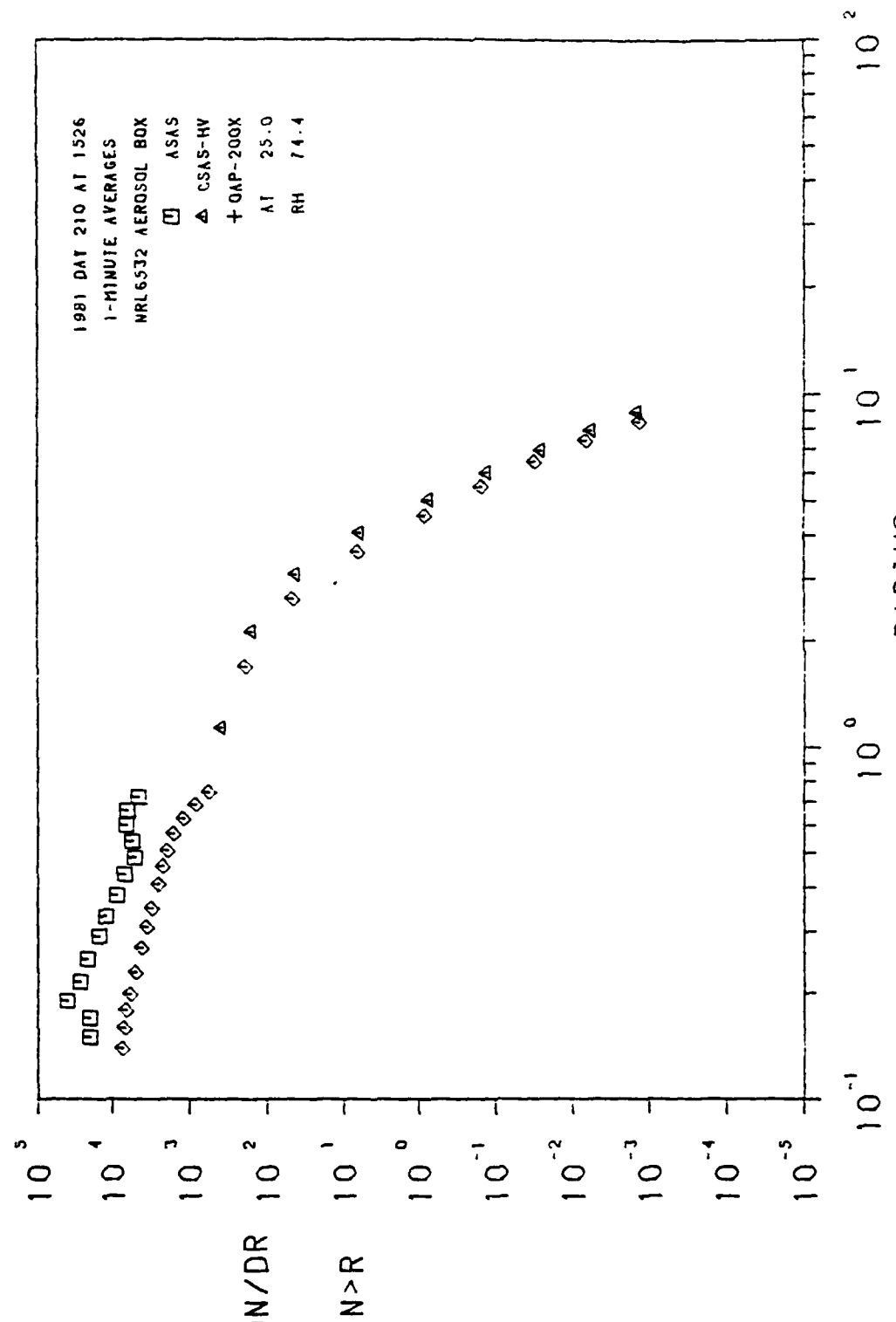

Fig. 28 — Particle size distribution for shot #741, no breakdown, 200 torr

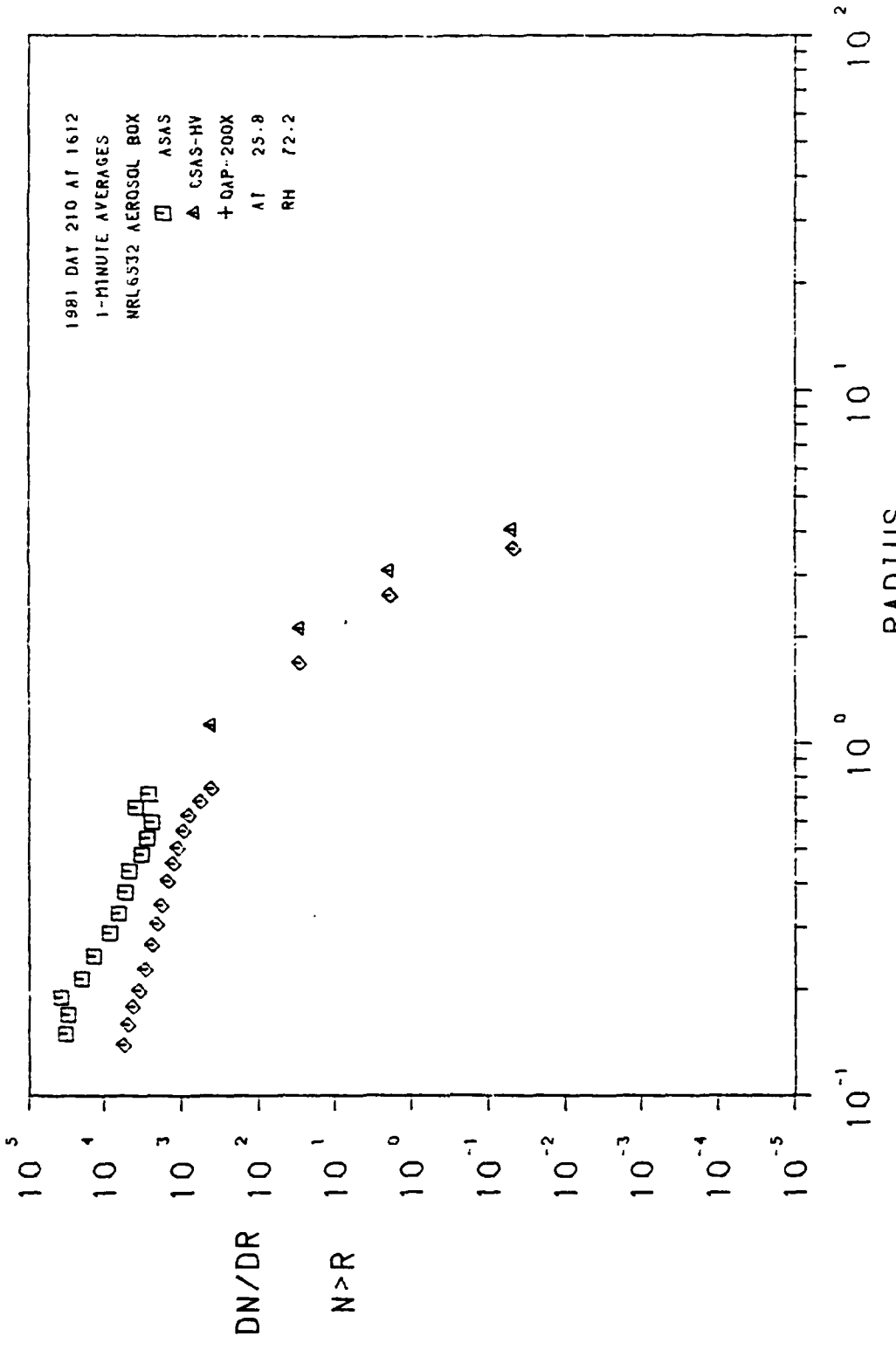

Fig. 29 — Particle size distribution for shot #743, breakdown, 225 torr

END

DATE
FILMED
4-82

DTIC